

Spectral elements numerical simulation of the 2009 L'Aquila earthquake on a detailed reconstructed domain.

F. Di Michele^a, J. May^b, D. Pera^b, V. Kastelic^c,
M. Carafa^c, C. Smerzini^d, I. Mazzieri^e, B. Rubino^b,
P. F. Antonietti^e, A. Quarteroni^{e,f}, R. Aloisio^{a,g}, P. Marcati^a

^a Gran Sasso Science Institute (GSSI), via M. Iacobucci 2, 67100 L'Aquila, Italy

^b Department of Information Engineering, Computer Science and Mathematics

University of L'Aquila, via Vetoio, loc. Coppito, I-67100 L'Aquila, Italy

^c Istituto Nazionale di Geofisica e Vulcanologia, Sezione Tettonofisica e Sismologia, L'Aquila, Italy

^d Department of Civil and Environmental Engineering, Politecnico di Milano, Piazza L. da Vinci 32, 20133 Milano, Italy

^e MOX - Dipartimento di Matematica, Politecnico di Milano, P.zza Leonardo da Vinci 32, 20133 Milano, Italy

^f Mathematics Institute, École Polytechnique Fédérale de Lausanne, Av. Piccard, CH 1015, Lausanne, Switzerland, Professor Emeritus

^g INFN-Laboratori Nazionali del Gran Sasso, Via G. Acitelli 22, Assergi (AQ), Italy

Received -; in original form -

SUMMARY

In this paper we simulate the earthquake that hit the city of L'Aquila on the 6th of April 2009 using SPEED (SPectral Elements in Elastodynamics with Discontinuous Galerkin), an open-source code able to simulate the propagation of seismic waves in complex three-dimensional (3D) domains. Our model includes an accurate 3D reconstruction of the Quaternary deposits, according to the most up-to-date data obtained from the Microzonation studies in Central Italy and a detailed model of the topography incorporated using a newly developed tool (May et al. 2021).

The sensitivity of our results with respect to different kinematic seismic sources is investigated. The results obtained are in good agreement with the recordings at the available seismic stations at epicentral distances within a range of 20km. Finally, a blind source prediction scenario application shows a reasonably good agreement between simulations and recordings can be obtained by simulating stochastic rupture realizations with basic input data. These results, although limited to nine simulated scenarios, demonstrate that it is possible to obtain a satisfactory reconstruction of a ground shaking scenario employing a stochastic source constrained on a limited amount of ex-ante information. A similar approach can be used to model future and past earthquakes for which little or no information is typically available, with potential relevant implications for seismic risk assessment.

Key words: Computational seismology – Earthquake ground motions – Earthquake hazards – Neotectonics – Site effects – Seismic wave propagation.

1 INTRODUCTION

Seismic damage and loss scenarios in large urban areas represent a key tool for civil protection planning to improve earthquake preparedness, establish effective prevention policies for seismic risk mitigation and support decision making in emergency management. To accomplish this task, a realistic estimation of earthquake ground motion and its spatial distribution during simulated earthquakes is essential, especially in the case of complex urban environments located close to seismically active faults. It is recognized that the coupling of seismic source features, geo-morphological structures and local site conditions, may have a dramatic influence in determining an uneven spatial distribution of ground shaking and, therefore the observed damage for homogeneous vulnerability conditions (Kawase 1996; Assimaki et al. 2012; Gallipoli et al. 2012). The standard approach for producing ground shaking scenarios during possible future earthquakes is the empirical approach, based on the use of Ground Motion Prediction Equations (GMPEs). GMPEs are statistical regressions on datasets of ground motion recordings, providing estimates of the probability distribution of ground motion intensity measures (e.g. Peak Ground Acceleration - PGA), as a function of explanatory variables, such as magnitude, distance and site conditions. GMPEs are routinely used in engineering practice but suffer because of the scarcity of data in the near-source region of severe earthquakes; the unsuitability to account for the specificity of the geological conditions; the spatial variability of ground motion. More recently, thanks to

the enormous computational capabilities made available by high-performance parallel computers, three-dimensional physics-based mathematical models have been extensively used to generate earthquake scenarios that account for the fault rupture and complexity of regional or local geological conditions (Burstedde et al. 2013; Petersson & Sjögreen 2018; Breuer et al. 2014; Galvez et al. 2014; van Zelst et al. 2019; Infantino et al. 2020; Paolucci et al. 2021a). These models rely on the numerical solution of the visco-elastodynamics equations in complex heterogeneous media with *high-order* and *flexible* computational methods, such as the Spectral Element Method (SEM) either in its continuous or discontinuous form, the ADER-DG method and the Finite Difference method to cite a few (Dumbser et al. 2007; Moczo et al. 2011; Pelties et al. 2012; Moczo et al. 2014; Chaljub et al. 2015; Antonietti et al. 2018; Duru et al. 2020; Wolf et al. 2020).

Because of the intrinsically high epistemic uncertainties involved in the construction of 3D numerical models, those need to be verified and validated against available earthquake recordings (Bielak et al. 2010; Paolucci et al. 2015, 2021b).

It is worth recalling that, owing to the considerable increase of earthquake recordings, state-of-the-art GMPEs begin to remove the ergodic assumption (i.e., equivalence between the distribution of the random variable in space and the distribution of the same variable at a single point when sampled over time) and, therefore, to mimic the physics-based simulations, by adjusting the model coefficients based on region-specific earthquake, path and site observed effects (Kotha et al. 2020; Sgobba et al. 2021). In this paper, the case study of the Mw 6.1 6th April 2009 earthquake which struck the city of L'Aquila (Abruzzo, Italy) causing 309 deaths and more than 1600 injuries, is addressed. L'Aquila was partially destroyed and so were many surrounding towns and villages. The main seismic event was preceded by a long sequence of fore-shocks (Sugan et al. 2014) and followed by hundreds of aftershocks, the largest of which occurred on the 7th April 2009 with a magnitude of 5.6. For this reason a dense set of seismic instruments was activated within the region, providing a unique amount of data in terms of number and quality (Ameri et al. 2009; Magnoni et al. 2013; Zambonelli et al. 2017), that was used to build relatively few 3D physics-based numerical simulations of the main event, cf. (Smerzini & Villani 2012; Magnoni et al. 2013; Evangelista et al. 2017).

In Magnoni et al. (2013) the authors reconstructed a large 3D domain which extends for 200km in the directions North-South (N-S) and East-West (E-W), with a depth of 60km. The Moho discontinuity as well as the main basins, such as Aterno and Fucino valley, were included. Simulations were made using SPEC3D.Cartesian software Komatitsch et al. (2004); Tromp et al. (2008); Peter et al. (2011) and the kinematic sources were taken from Cirella et al. (2009). These results were in good agreement with the 27 recorded signals in the frequency range 0.02 – 0.5 Hz.

In Smerzini & Villani (2012) the same earthquake was simulated on a domain with dimensions around 62 km in N-S and E-W directions and 20 km depth. Numerical results were obtained with GeoELSE (Stupazzini et al. 2009) by comparing four

kinematic sources coming from the inversion of seismic data, at frequencies up to 2.5 Hz. As in the previous case the synthetic seismographs were compared to the recorded data, and a fairly good agreement was observed. More recently in Evangelista et al. (2017) the authors simulate the April 9, 2009 earthquake using a comparable domain and a similar approach as in Smerzini & Villani (2012), using a more recently developed library named SPEED that is based on a discontinuous Galerkin Spectral Element paradigm (Antonietti et al. 2012; Mazzieri et al. 2013). The more accurate reconstruction of the alluvial basin and of the kinematic source allows for a better agreement with the recorded data with respect to Smerzini & Villani (2012).

In this work, we present a new set of numerical simulations of the L'Aquila event, using the same numerical code SPEED. Some improvements were made to the pre-processing MATLAB scripts in order to correctly handle the newer versions of the exodus file type, seen in (at least) Trelis 16.3 (now Coreform Cubit <https://coreform.com/products/coreform-cubit>). The new numerical model of the L'Aquila area was obtained, by focusing on the following aspects: (i) the subsoil reconstruction, with emphasis on the Middle Aterno Valley - a Quaternary sedimentary basin - on which L'Aquila town is built; (ii) the topography reconstruction with inclusion of high mountains and canyons that could influence wave propagation; and finally, (iii) the influence of the kinematic source. Comparing with the models available in literature (Magnoni et al. 2013; Smerzini & Villani 2012; Evangelista et al. 2017), our reconstructed domain follows the geological and morphological characteristics of the investigated area with a higher accuracy. To create the topography of the computational domain, we started from a 10 m resolution DEM provided by the TINITALY project (see Tarquini et al. (2007, 2012); Tarquini & Nannipieri (2017) for more details) and, using a new software tool, cf. May et al. (2021), we achieved a highly accurate reconstruction. This procedure requires minimal user input and interfaces directly with the Trelis/Cubit software. The importance of using an accurate topography has been emphasized in Magnoni et al. (2013) and in many other papers, see for example (Bouchon et al. 1996; Bouchon & Barker 1996; Durand et al. 1999; Lee et al. 2009).

The influence of the kinematic seismic source on earthquake ground motions in the near-source region is explored by considering both the source inversion models presented in Atzori et al. (2009); Ameri et al. (2012); Evangelista et al. (2017) and sources computed with the stochastic rupture generator by Schmedes et al. (2013).

The paper is organized as follows. In Section 2 we describe the domain creation procedure and present the geological setting on which the computational domain is built, emphasizing the contribution to the available literature. In Section 3 we discuss the effect of different seismic sources for the simulation of the April 6, 2009 L'Aquila earthquake. In particular we compare two kinematic sources obtained by different techniques for seismic source inversion. Results of the simulations are discussed and the comparison with the available recorded data is shown. Finally, in Section 4 we perform a "blind prediction" exercise. To this

end, the 2009 earthquake is simulated using a stochastic co-seismic slip distribution (Schmedes et al. 2013), across an assigned fault plane according to the Database of Individual Seismogenic Sources - DISS (<http://diss.rm.ingv.it/dissGM/>). The comparison between the synthetic scenarios and recorded data is addressed, in order to evaluate the prediction capability of the simulations with a source model constrained on a limited input information. In the final section we draw some conclusions and illustrate possible future developments of this work.

2 SIMULATION DESIGN: GEOLOGICAL SETTING AND COMPUTATIONAL DOMAIN CONSTRUCTION

In this section we show the construction of the computational model, obtained starting from a detailed topography reconstruction and a large-scale 3D model of the Quaternary-infill of the area of interest. Moreover, we present a new tool able to simplify and speed up the construction of the computational mesh, cf. May et al. (2021).

2.1 Geologic setting and Quaternary basin reconstruction

It is well known that the basin geometry and its overall structure and composition influence the lateral variations in peak earthquake ground motion, amplification and shaking duration (Gutenberg (1957); De Luca et al. (2005); Ewald et al. (2006)). As the scope of the present work is to reproduce the ground shaking in a given area as accurately as possible, we strive to include in our numerical model not only realistic seismic sources but also a detailed reconstruction of the submerged morphology of the territory. With respect to the previous works that consider the same study area (e.g. Smerzini & Villani (2012); Evangelista et al. (2017)), we aimed to construct a more spatially and geometrically comprehensive numerical model based on numerous geologic, geophysical and geomorphologic data.

Our study area is situated in the central Apennines, a mountain chain characterized by post-collisional seismogenic active extension predominantly expressed along NW-SE striking normal faults and by regional-scale uplift. The seismogenic normal faults rejuvenate the older compressional tectonic-related setting (e.g., Patacca & Scandone (1989)) and affect the Meso-Cenozoic carbonate and partially terrigenous rocks, while their activity controls the deposition and deformation of Quaternary sediments in their form of basin infill (e.g., Bosi (1989); Centamore et al. (2010)). The typical morphology of the central Apennines consists of individual NW-SE oriented mountain fronts and intermediary high karstic plateaus intermittent with inter-mountain basins and fluvial-glacial valleys. Such morphology is the outcome of different tectonic phases that affected the area during its geological evolution (Bertini & Bosi 1976), as well as effects of gravity driven displacements in the form of

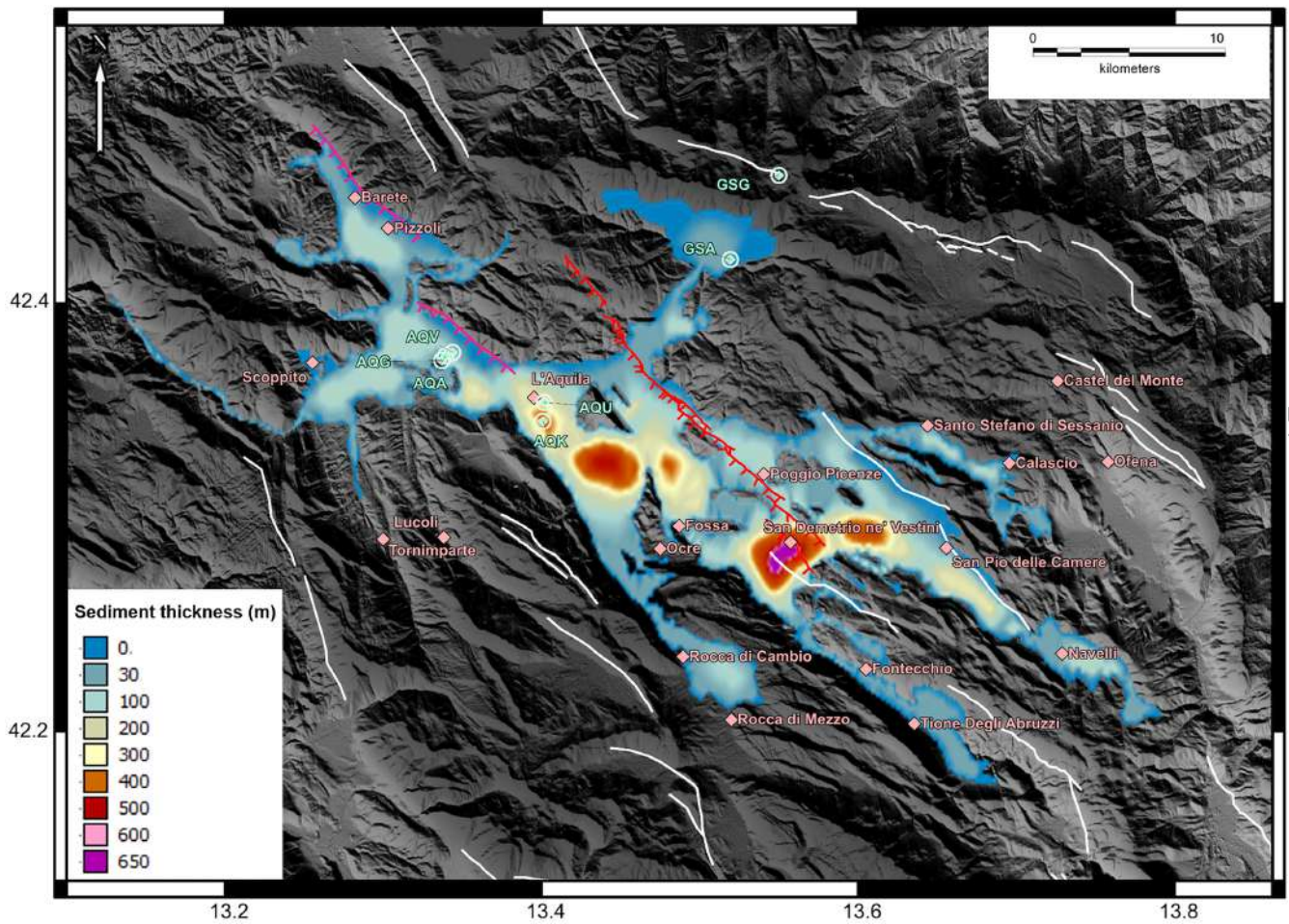


Figure 1. Map of the Quaternary L'Aquila – San Demetrio sedimentary basin. The white polylines represent local active faults (from Carafa et al. (2020)). The red (Paganica – San Demetrio) and magenta (Pizzoli – Mt. Marine) are active faults that are discussed in Section 2.1. The green textured circles represent the seismic stations used in the analyses (from table 2). For more details, see the text.

slope instabilities, landslides and different erosion processes (e.g. (Della Seta et al. 2017; Kastelic et al. 2017)). In the current geodynamic setting, the area is subjected to regional extension of 2-3 mm/yr (Carafa & Bird 2016; Carafa et al. 2020). The effective seismogenic deformation likely represents about 70% of the total regional tectonic extension (Carafa et al. 2017) and is expressed also in the form of strong earthquakes, as is the case of 1915 Fucino event, one of the strongest earthquakes ever recorded in the Italian territory (Guidoboni et al. 2019; Rovida et al. 2019).

The broader L'Aquila area is positioned in the Upper and Middle Aterno inter-mountain fluvial basin (UMAB) between the Gran Sasso and Mt. Sirente-Mt. Cefalone mountain ridges (Figure 1). Besides the ongoing regional uplift, the zone was subjected to compression expressed along the respective thrust faults that created the high topography terrain and related lower-terrain foredeeps. The activity of younger, leading extensional faults in the UMAB, namely the SW-dipping Monte Marine-Pettino and Paganica-San Demetrio extensional fault systems (drawn in magenta and red in figure 1) further

pronounced the topographic difference accentuating the basin depth and simultaneously creating new depositional environment of lacustrine-palustrine to fluvial to alluvial origin.

The UMAB is heterogeneous in its depth and lithological composition. In fact, it is usually described as two distinct basins with NW sector referred to as L'Aquila – Scoppito basin and the SE sector commonly known as the Middle Aterno Valley. The basin itself is interrupted by several intrabasin highs composed of carbonatic or terrigenous bedrock. The UMAB area corresponds to epicenter location of various Mw (or Me) ≥ 5.5 earthquakes, namely the 2nd February 1703; 3rd December 1315; 27th November 1461; 6th October 1762; and the 6th and 7th April 2009 earthquakes (Guidoboni et al. 2019; Rovida et al. 2019) that all caused rather extensive damage through its territory.

We based the reconstruction of the 3D basin on available data from geological maps (Vezzani et al. 1998; Dipartimento Difesa del Suolo 2005a,b,c; Servizio Geologico d'Italia 2010a,b), borehole data (Porreca et al. 2016), well logs (Nocentini et al. 2017; Cosentino et al. 2017), seismic profiles (Improta et al. 2012; Tallini et al. 2012), deep electric resistivity surveys (Balasco et al. 2011; Pucci et al. 2016) and their interpretations. We further coupled the above mentioned material with results of microzonation investigation conducted in the broader L'Aquila territory after the 2009 earthquake, the seismic microzonation of the L'Aquila territory project (MS-AQ Working Group and others 2010).

The external borders of the UMAB basin were mapped in order to respect the surface extension of Quaternary lithology, that is the areas where the Quaternary rock or sediment thickness is above zero meters. The spatial extension of the UMAB is from the Campo Imperatore to the N and the Altopiano delle Rocche to the S. We aimed to include in the main basin also the more important fluvial valleys which are influenced by a continuous extension of alluvium, like the Valle del Salto at the basin W extension.

Besides the basin extension limit where the Quaternary infill thickness is set to zero, we, based on the retrieved data, mapped a further six isolines corresponding to 30, 115, 225, 400, 480 and 640 red meters Quaternary infill thickness. These values were chosen based on the geometry of the basin along the sections with the best data coverage, considering the overall distribution of the basin infill thickness. Starting from the points with known infill thickness we can interpolate the parameter values for the entire basin extension through a triangulation approach. The SE UMAB sector is larger and deeper with respect to its NW counterpart. The greatest infill thickness of 640 m is reached in the San Demetrio area, the portion of the UMAB with greatest gradients in the basin geometry. The local high in the basin geometry separates the deepest basin section from its NW continuation, where infill thickness reaches 400 meters. Local depocenters where infill thickness reaches or surpasses 400 m of smaller dimensions are present also in the central part of the UMAB. The SE sector is composed of three different synthems (Giaccio et al. 2012; Nocentini et al. 2018), while in the NW sector two different depositional events were recognized

Table 1. Crustal model coefficients.

<i>Layer</i>	<i>Depth (km)</i>	V_S (m/s)	V_P (m/s)	ρ (g/cm ³)	Q
1	1	1700	3160	2.5	100
2	1	2600	4380	2.5	200
3	3	3100	5760	2.84	200
4	15	3500	6510	3.18	200

(Mancini et al. 2012). The first basin infill consists of talus breccias and slope-derived breccias, debris-flow deposits, and alluvial clayey-sandy conglomerates (Bertini & Bosi 1993; Cosentino et al. 2017). The lacustrine sedimentary units, mainly composed of calcareous silts, clays, lignite and occasionally also tephra layers (Bosi & Bertini 1970; Centamore et al. 2010; Nocentini et al. 2018), are recognized in the deeper basin sectors. Laterally the lacustrine units pass to heterogeneous delta type sedimentation of coarser grained units. During its evolution the depositional environment passed to more palustrine sedimentation type environment influenced also by local erosion that caused the presence of coarser sandy to conglomeratic material in between a finer grained silts (Macrì et al. 2016). Progressively the environment passed to prevailing fluvial-alluvial derived mid to coarse grained sedimentation type, many times organized in the form of fluvial terraces (e.g., Nocentini et al. (2018)). The youngest basin infill is represented by the Holocene fluvial, colluvial, scree deposits and landslides (e.g., Dipartimento Difesa del Suolo (2005a); Centamore et al. (2010)) related to the erosional and depositional processes still active in the UMAB basin.

The detailed basin reconstruction was designed with the scope of improving our knowledge on the basin subsurface characteristics, keeping in mind that wave propagation and local ground motion amplification are controlled mainly by geometric complexities in the buried bedrock topography and seismostratigraphic properties of the sedimentary infill (Bard & Bouchon 1980; De Luca et al. 2005).

A homogeneous linear visco-elastic seismo-stratigraphic profile has been assumed for the alluvial deposits inside the Aterno valley, according to (Evangelista et al. 2017):

$$V_S = 300 + 36 \cdot z^{0.43} \text{ (m/s)}, \quad V_P = V_S \sqrt{4.57}, \quad Q_S = 0.10V_S, \quad \rho = 1.9 \text{ (g/cm}^3\text{)}. \quad (1)$$

where z denotes the depth from the topographic surface, V_S the shear wave velocity, V_P the compressional wave velocity, ρ the soil mass density, and Q_S the S-wave quality factor defined from the V_S profile. Outside the Aterno valley, a horizontally layered crustal model is assumed as in Table 1 (see Ameri et al. (2012); Evangelista et al. (2017) and references therein for more details)

2.2 Automated domain reconstruction software

In this work, a high-resolution topography was considered during the generation of the computational grid. The importance of having an optimal topography representation for physics-based numerical simulations has been considered several times, we refer, for example, to (Lovati et al. 2011; Hailemikael et al. 2016; Asimaki & Mohammadi 2018) and references therein. Different reconstruction techniques have been employed to define the Earth surface starting from geo-referenced data. Depending on the area of interest and on the level of accuracy required, a surface reconstruction may take anything from minutes to days to create, requiring constant human inputs. Moreover, careful selection of the programming language used is required in order to provide outputs compatible with the software employed for the mesh generation: in our case Coreform Cubit (<https://coreform.com/products/coreform-cubit>).

In order to simplify the construction of an accurate Earth's surface as well as a three dimensional computational domain in a quick and simple way, while requiring minimal input, we have designed a set of Python (<https://www.python.org/>) scripts which interface directly with Coreform Cubit. These scripts allow for the creation of: *i*) a topographical surface of any size; *ii*) a cake-layered three dimensional domain; *iii*) a given number of fault planes to be included in the model, cf. Figure 2.

The scripts require users inputs at the initial step and then proceed to generate the domain in an automatic way. This allows the creation of several distinct domains in a simple, time effective manner in parallel.

An overview of the workflow we have designed to build a computational model in Coreform Cubit is summarized in Figure 2.

A more detailed explanation, as well as timing examples, can be found in May et al. (2021).

3 PARAMETRIC STUDY ON THE KINEMATIC SEISMIC SOURCE

In the previous section we outlined the procedure used to obtain a detailed reconstruction of the geo-morphological structure of the study area (basin and topography). However a well-constrained model for a seismic source is crucial to obtain accurate results, especially in the near-source region where ground motion features are governed by the details of the fault rupture process. Within this paper the seismic source is represented by a kinematic model on a prescribed fault defined geometrically by a plane, approximating the real fault structure.

The aim of this subsection is to compare the numerical results obtained by using two kinematic sources, retrieved from the finite-fault solutions available from literature studies for the Mw 6.3 April 6, 2009 earthquake. The sources are obtained using two different techniques, one from the inversion of the recorded ground motions and the second one employing the DInSAR technique. This choice has been done with the aim of comparing the impact of the two approaches for source inversion on the

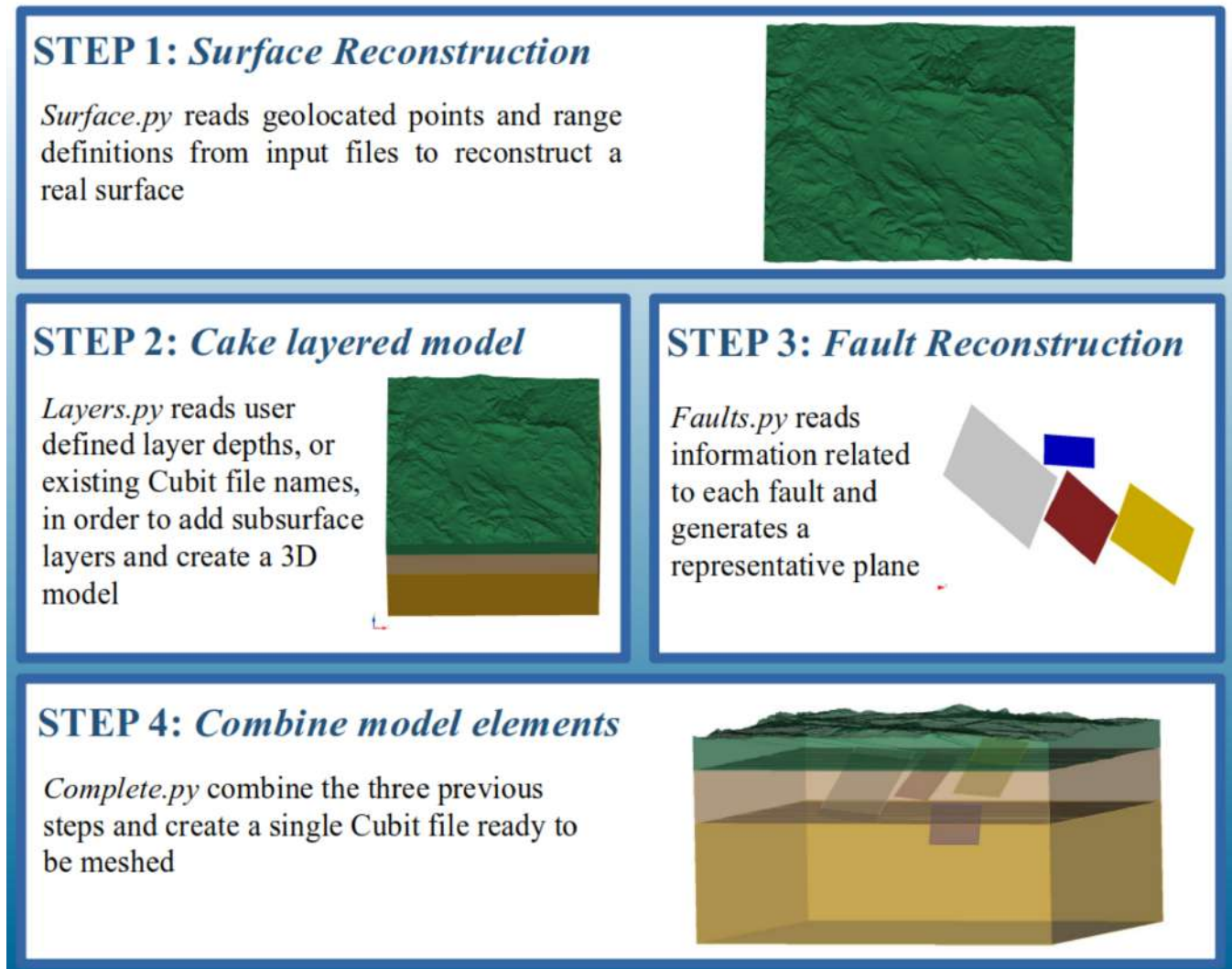


Figure 2. Schematic description of the Python scripts workflow.

results of physics-based 3D simulation. Note that, for each kinematic source, a 3D mesh has been constructed that matches exactly the geometry of the fault plane. The kinematic source models adopted as well as the computational domains considered are provided in Figure 3 and Figure 4, respectively.

All simulations discussed in this work are done using the code SPEED. In this numerical tool, the viscous elastodynamic equation, describing the soil displacement, is approximated using the discontinuous spectral element method in space coupled with the leap-frog scheme in time. SPEED allows one to use non-conforming meshes and different polynomial approximation degrees in the numerical model. This makes mesh design more flexible (since grid elements need not match across interfaces) and permits the selection of the best-fitting discretization parameters in the computational domain, while controlling the overall accuracy of the approximation. More specifically, the numerical mesh may consist of smaller elements and low-order polynomials where wave speeds are slowest, and of larger elements and high-order polynomial where wave speeds are fastest.

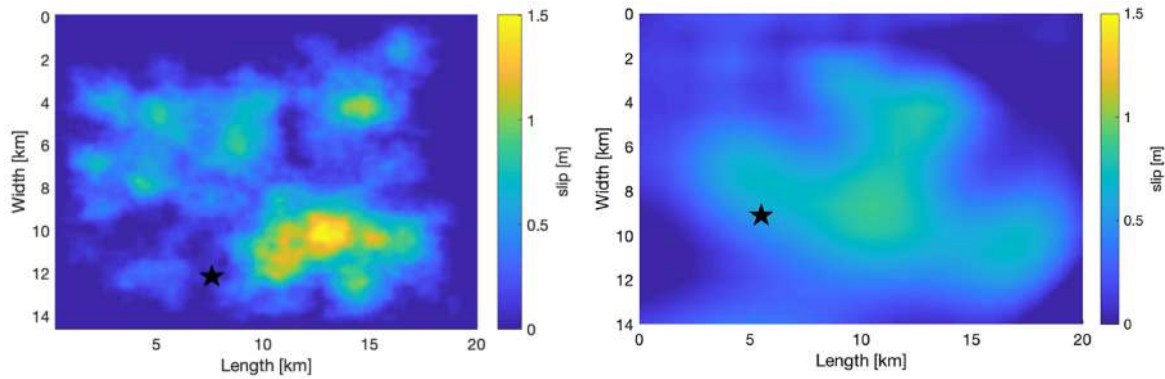


Figure 3. Slip distribution on the implemented coseismic fault plane for *Model 1* (left) and *Model 2* (right).

We refer the reader to Antonietti et al. (2012, 2016); Ferroni et al. (2017) for the analysis of the scheme, to Mazzieri et al. (2013) for implementation details and to Smerzini & Villani (2012); Paolucci et al. (2015, 2016); Infantino et al. (2020); Paolucci et al. (2021a) for other relevant applications in computational seismology.

The first source, constructed by Ameri et al. (2012), has been obtained by inverting strong ground motion data and it has previously been used in Evangelista et al. (2017) on a different 3D computational model. Details about the kinematic source and fault geometry can be found in Figures 3-(left) and 4-(a), respectively. Rise time and rupture velocity are randomly distributed around mean values of 0.7s and 2500m/s, respectively.

The second kinematic source has been provided from Atzori et al. (2009) and it has been derived by DInSAR technique using the images of permanent displacement provided by ENVISAT and COSMO–SkyMed satellites. The slip values, assigned on the fault plane, are not constant and reach a maximum value of approximately 90cm (see Figure 3-(right)). The geometric parameters of the fault are summarized in Figure 4-(b). Rise time and rupture velocity distribution are assumed to be constant, i.e., 0.7 s and 2500 m/s, respectively. Hereafter the *Ameri et al.* and *Atzori et al.* source models are referred to as *Model 1* and *Model 2*, respectively.

Many other slip distributions are available in literature. See, for example, Yano et al. (2014); Cheloni et al. (2010); Avallone et al. (2011) and references therein.

The grids considered for *Model 1* and *Model 2* have approximately $8 \cdot 10^5$ and $40 \cdot 10^5$ nodes, respectively. Both meshes are able to propagate frequencies up to approximately 2.5 Hz, cf. Figure 4. The simulation of *Model 1* took approximately 14 hours walltime, with time step 0.0005s and final time $T = 30$ s, on two nodes consisting of DELL R730 2 CPUs Intel Xeon E5-2698 2.20GHz, RAM 256Gb using (18022a MPI-threads) installed on Caliban Cluster (<https://caliband.disim.univaq.it>). *Model 2* simulations took 60 hours walltime, with time step 0.00025s and final time $T = 30$ s, on one node containing HP Proliant DL 580 Gen 10 with 4 CPUs Intel Xeon Gold 6140M 2.30GHz, RAM 512Gb using (140 MPI-threads) on Caliban Cluster. To

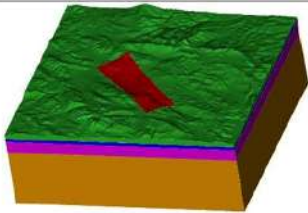
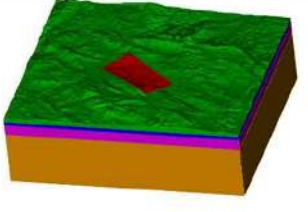
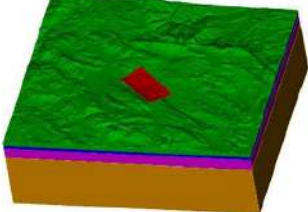
<i>Model</i>	<i>Fault Solution</i>	<i>Mw</i>	<i>Slip distribution</i>	<i>Mesh Features</i>	<i>Domain Image</i>
Model 1	L = 28 km W = 20.9 km Strike = 133° Dip = 54° Rake = -102°	6.1	1	Size = (59.5, 57.5, 19.8) km No. Elements = 776426 Spectral Degree = 3 No. mesh nodes = 803222 $\Delta t = 0.0005s$ Duration = 30s	
Model 2	L = 20 km W = 14 km Strike = 133.5° Dip = 47° Rake = -103.5°	6.3	1	Size = (65.9, 57.8, 19.8) km No. Elements = 3762721 Spectral Degree = 3 No. mesh nodes = 4088818 $\Delta t = 0.00025s$ Duration = 30s	
Paganica Prediction	L = 14 km W = 9.5 km Strike = 127° Dip = 50° Rake = 270°	6.1 6.2 6.3	3 (hypothetical) 3 (hypothetical) 3 (hypothetical)	Size = (65.9, 57.8, 19.8) km No. Elements = 1715476 Spectral Degree = 3 No. mesh nodes = 1865398 $\Delta t = 0.00025s$ Duration = 30s	

Figure 4. Description of the three computational domains, labeled as *Model 1*, *Model 2* and blind prediction. For each of them, size, mesh properties, related fault plane and the magnitude of the simulate earthquake(s), are displayed. Each fault projection is shown in red.

validate the computational models, we compare our results with the available near-source recordings located within 20 km of epicentral distance, see Table 2.

In Figures 5 and 6 snapshots of the horizontal (EW) velocity wavefield simulated by SPEED at four different times are shown for the *Model 1* and the *Model 2*, respectively. In the first panel we can observe the initiation of the rupture, consistently

Table 2. Position of the seismic stations, in terms of geographic coordinates, Lat(°N) - Lon (°E), and epicentral distance (R_e).

Seismic stations ID	Lat (°)	Long (°)	R_e (Km)
AQK	42.3449	13.4009	1.8
AQU	42.3538	13.4019	2.2
AQV	42.3772	13.3438	4.9
AQG	42.3734	13.3370	5.0
AQA	42.3755	13.3392	5.0
GSA	42.4206	13.5193	14.4
GSG	42.4600	13.5500	19.2

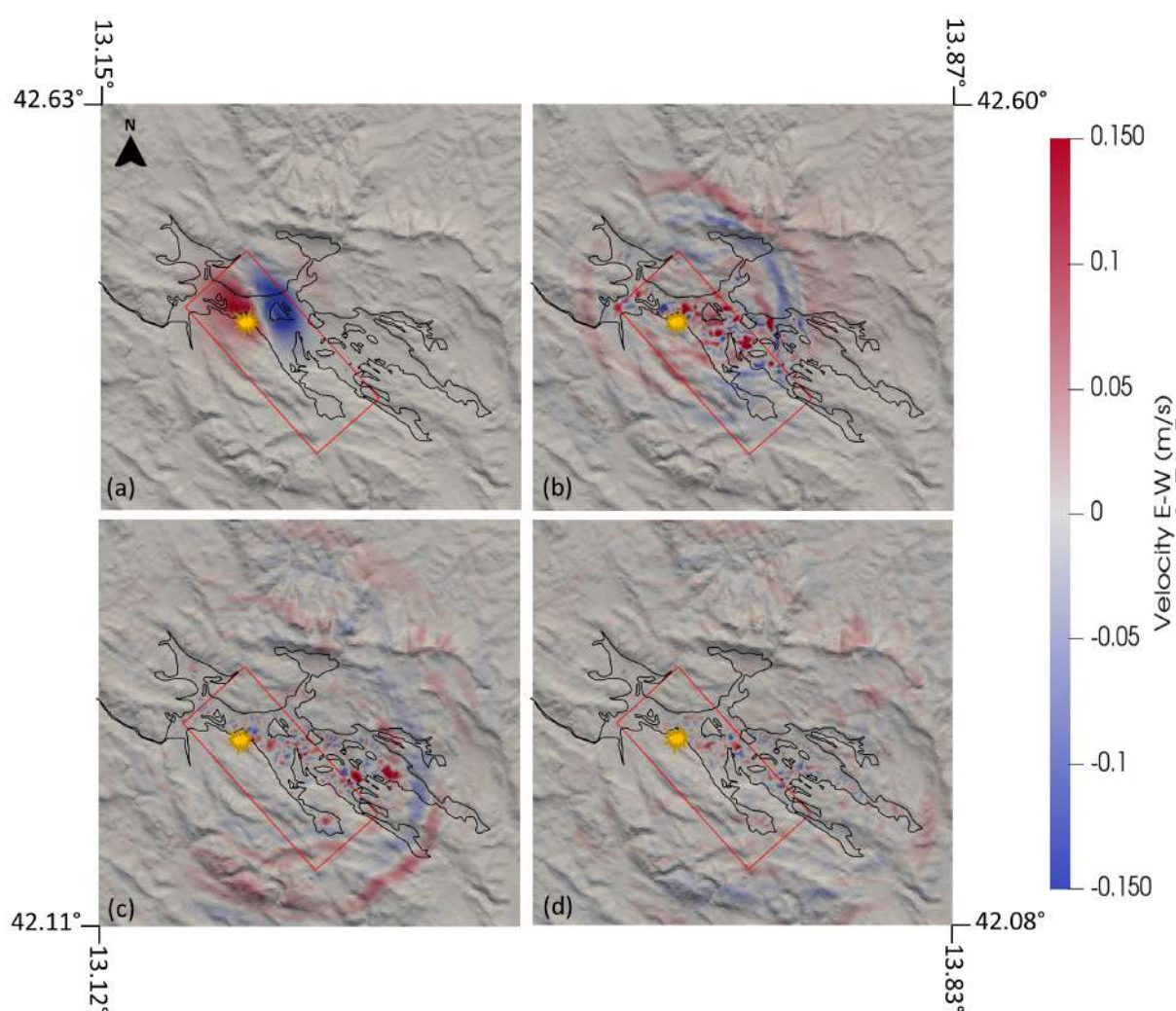


Figure 5. Velocity in the EW direction (m/s) for Model 1 at 6, 10, 16 and 20s (a, b, c, d, respectively).

with the assumed focal mechanism (normal), whereas in the subsequent panels the trapping of seismic waves inside the basin is apparent. In Figure 7 the time histories of displacement and velocity waveforms simulated at three stations, namely, AQK, AQU and AQG (see Table 2) are shown and compared with the recorded ones, for the three components of motion (East-West (EW), North-South (NS) and Up-Down (UD)).

The agreement between recorded and simulated waveforms is rather satisfactory, both for the displacement and the velocity field, especially at the stations AQK and AQU, with good fit in terms of first arrivals, predominant frequencies and peak values. A poor agreement is found at AQG station, in particular for the NS component, with underestimation of simulations, most likely because of the lack of some asperities in the slip distribution across the fault towards the NW sector of the Aterno Valley as well as the simplified velocity model assumptions.

To have a quantitative evaluation of the performance of the numerical model, the goodness-of-fit (GoF) criteria introduced

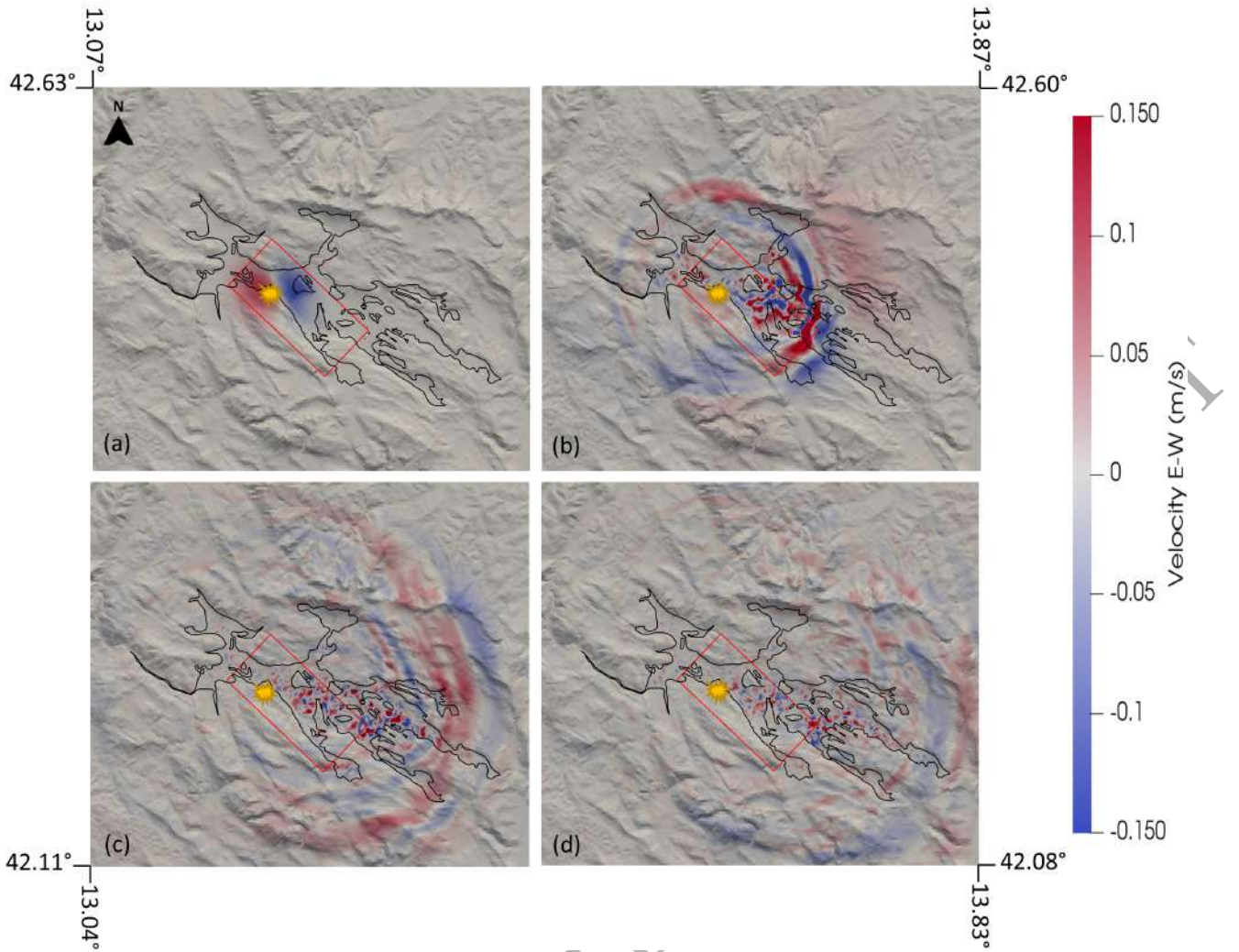


Figure 6. Velocity in the EW direction (m/s) for Model 2 at 4, 8, 14 and 18s (a, b, c, d, respectively).

by Anderson (2004) are evaluated. We recall that for each parameter a goodness-fit score ranging from 0 to 10 is assigned: 'poor fit' is obtained for values smaller than 4, 'fair fit' between 4 and 6, 'good fit' between 6 and 8, and 'excellent fit' between 8 and 10. Here, the GoF are computed considering five parameters, including integral, peak and spectral measures, regarded as the most significant from an engineering point of view, namely: *Energy Duration* (ED), *Peak Ground Velocity* (PGV), *Peak Ground Displacement* (PGD), *Response Spectral Acceleration* (RSA) and *Fourier Amplitude Spectra* (FAS).

In the following, the simulated and recorded data will be referred to as s and r , respectively. We define

$$I_E(t) = \int_0^t v(s)ds, \quad (2)$$

$$ED = 10 \left[1 - \max \left(\left| \frac{I_{E_r}(t)}{I_{E_r}(T)} - \frac{I_{E_s}(t)}{I_{E_s}(T)} \right| \right) \right]. \quad (3)$$

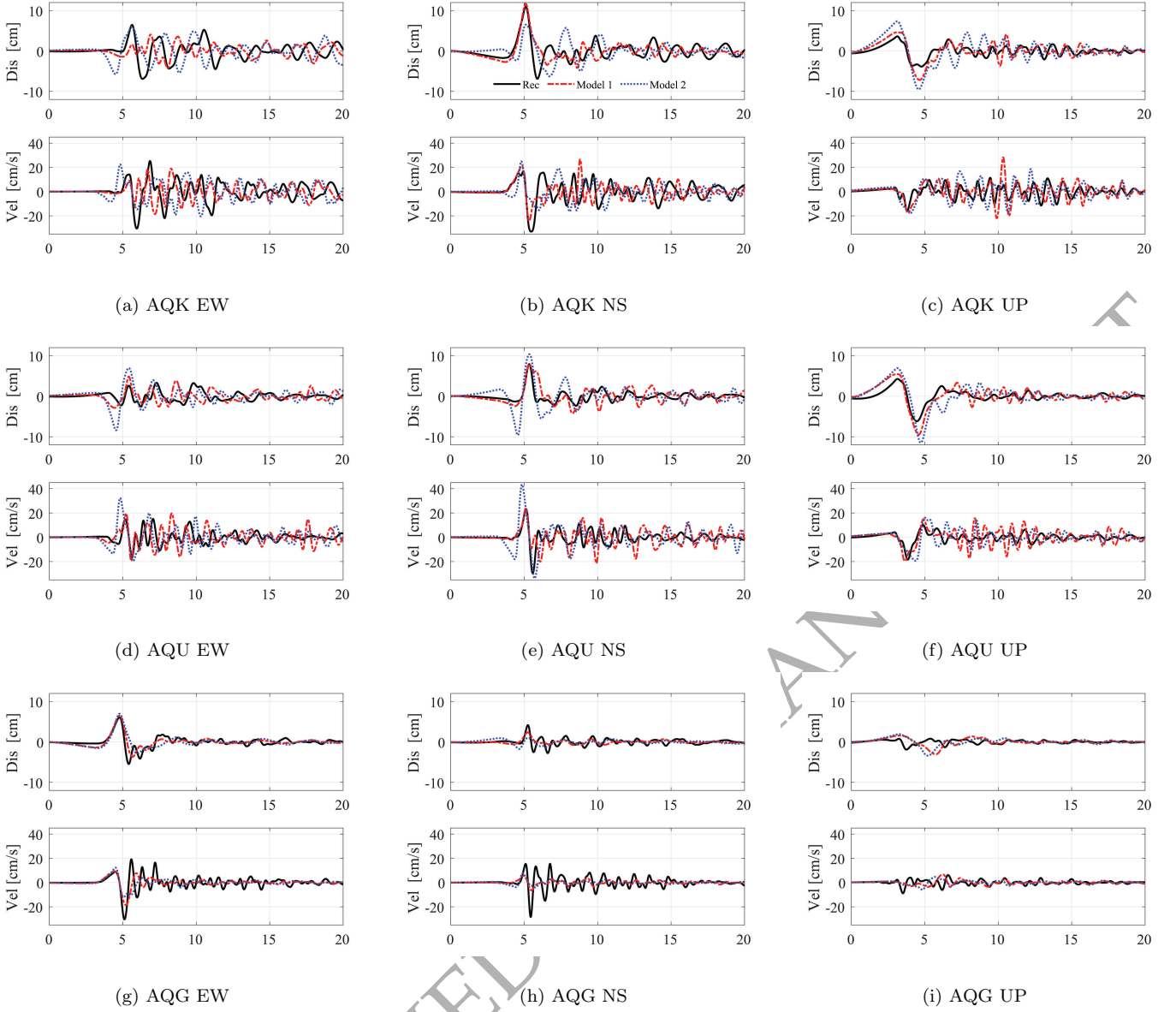


Figure 7. Comparison between the recorded (black lines) and simulated displacement and velocity waveforms for both *Model 1* (red lines) and *Model 2* (blue lines) sources at three stations: AQK, AQU and AQG (see Table 2), in the frequency range [0.1-2.5] Hz

$$PGV = S(|\max(v_r(t)) - \max(v_s(t))|) \quad PGD = S(|\max(d_r(t)) - \max(d_s(t))|) \quad (4)$$

$$RAS = \text{mean}(S(RAS_r(f) - RAS_s(f))) \quad FAS = \text{mean}(S(FAS_r(f) - FAS_s(f))). \quad (5)$$

Figure 8 shows the GoF scores obtained at the seven stations listed in Table 2 for the five aforementioned parameters, for both *Model 1* and *Model 2* source models (Figures 8-(a) and 8-(b), respectively). For each station the symbol shown indicates the average value obtained from the three components. Moreover, in Figure 8-(c) we report the scores obtained by averaging the five parameters with respect to each station. It turns out that the GoF is higher for *Model 1* than for *Model*

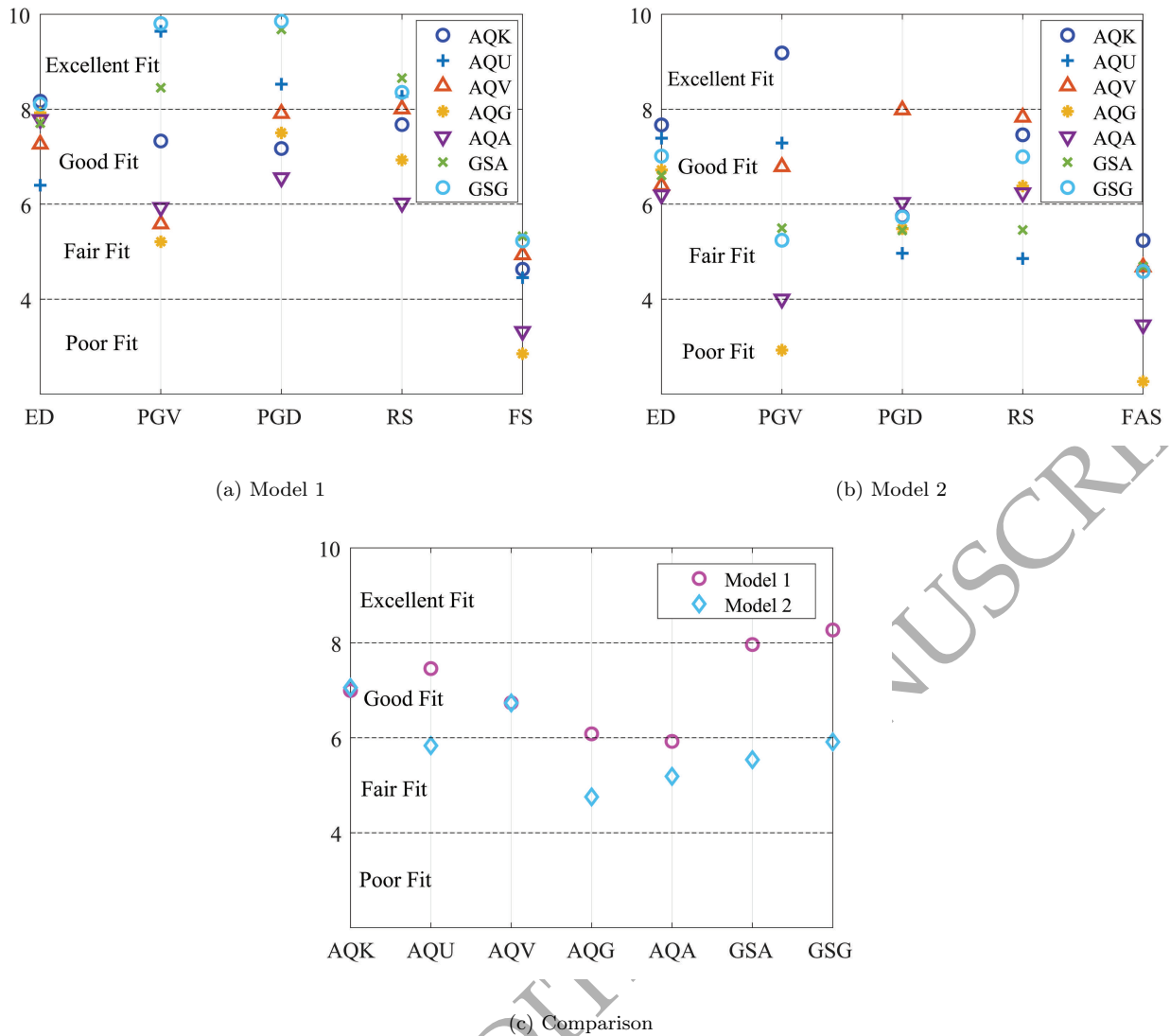


Figure 8. Goodness-of-Fit (GoF) scores at the seven stations listed in Table 2 for the frequency range [0.1-2.5] Hz for each of the five selected parameters. (a) shows Model 1, (b) Model 2 and (c) the comparison of average scores from the two source models.

2, at least in the considered range of frequencies. In particular we underline that for *Model 1* the average value of the five parameters is in the 'good fit' range for all the stations considered, except AQA, for which the GoF score is slightly less than the 'good fit' threshold, i.e. 6.0. Comparing these results with the ones present in literature, e.g., Smerzini & Villani (2012); Evangelista et al. (2017), we note an improvement of the overall GoF scores. Furthermore, from Figure 8(a)-(b) we can see that for both sources the scores associated with the ED parameter are between 6 (good) and 8 (excellent) for all stations, with limited dispersion. This suggests a good agreement between the recorded and simulated velocities, cf. Figure 7. As a further validation, in Figure 9 the modulus of the permanent displacement vector at the time instant = 30 s for both *Model 1* (a) and *Model 2* (b), is compared to the co-seismic displacement obtained by geodetic measurements (c) (courtesy of Simone Atzori, INGV). For both sources the largest displacement, of around 17.5 cm for *Model 1* and 25 cm for *Model 2*, is reached on the

hanging wall of the fault, a few kilometers SE of the epicenter. The source *Model 1* underestimates, by around 40 percent, the satellite deformation field, which is better described by *Model 2*, where maximum underpredictions of approximately 15 percent are found. This is expected since *Model 2* is based directly on the inversion of DInSAR data. These misfits can be attributed to the assumptions at the base of the kinematic source model, such as the regular, smooth geometry of the fault and the simplified 1D visco-elastic soil model considered for the inversion.

Finally, in Figure 10, we compare the PGV maps, obtained from our numerical simulations with the one provided in <http://shakemap.ingv.it/shake/archive/>. In our framework the PGV maps contain the maximum between the EW and NS components of the velocity. Note that the resolution of our model is around 2-2.5 Hz and PGV is typically associated with frequencies below this limit (see Paolucci & Smerzini (2018)), therefore the comparison with ShakeMaps can be expected, at first approximation, to show a reasonable good agreement. On the one hand *Model 1* reproduces quite well the measured PGV map. On the other hand *Model 2* tends to provide higher maximum PGV values.

4 “BLIND PREDICTION” TEST

In the previous section, we have shown a quantitative comparison between numerical simulations and recorded data of the Mw 6.3 April 6, 2009 L'Aquila earthquake. The former have been obtained using a detailed information about the seismic source, as well as detailed geophysical reconstruction of the Aterno valley. In this section we try to simulate the main event using basic information typically available a few minutes after the earthquake (magnitude, epicenter location and fault geometry). In other words, we made a kind of blind prediction exercise to explore to which extent the simulated scenario agrees with the observed ground motions, when little *a-priori* information on the event is available.

For this purpose, as basic input data, we considered: (i) the Paganica fault geometry, as provided in the Database of Individual Seismogenic Sources - DISS (<http://diss.rm.ingv.it/dissGM/>); (ii) the epicenter location at 42.34 Lat - 13.38 Lon with depth fixed at 9 km (value considered reasonable for seismic events occurring on the central Apennines having approximately Mw 6); and (iii) a magnitude Mw range from 6.1 to 6.3 to account for the typical uncertainty in magnitude estimation. Regarding the causative fault (i), it is worth recalling that the Paganica fault was not included in the DISS database prior to the L'Aquila earthquake. The Paganica fault extends for 14 km in length and 9.5 km in width; strike, dip and rake are 133°, 43° and 275°, respectively.

The details of the 3D computational domain adopted for these earthquake scenarios are summarized in Figure 4, on the third row. For each scenario earthquake associated with a prescribed magnitude level, we considered three different source

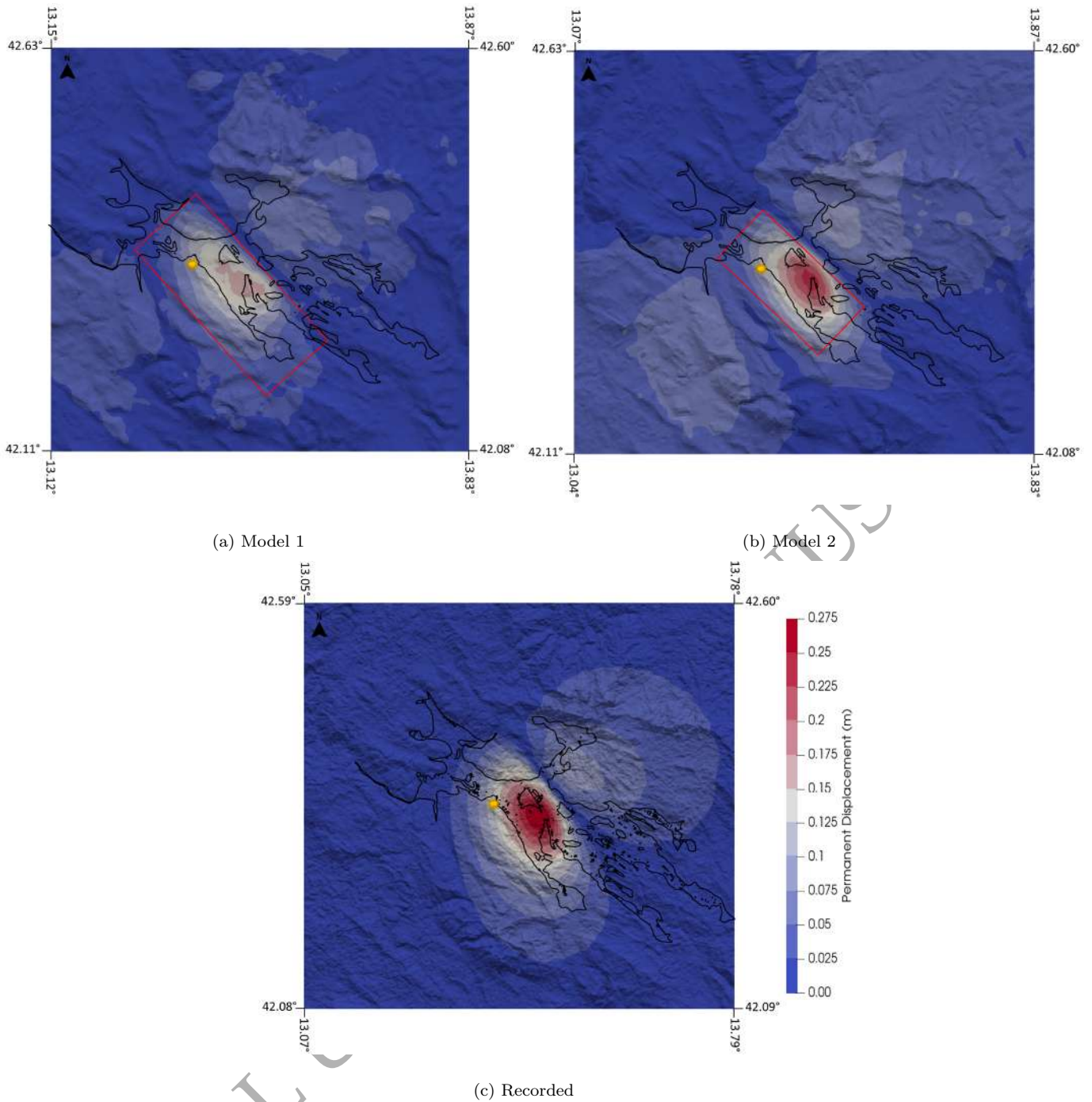


Figure 9. Modulus of the permanent displacement registered at 30s for source *Model 1* (a) and *Model 2* (b), compared to the co-seismic displacement obtained by satellite data (c) (courtesy of Simone Atzori)

rupture realizations, leading to a total of 9 simulations. The fault rupture realizations are generated using the kinematic model generated by Schmedes et al. (2013). Figure 11 illustrates the 9 slip distributions considered for these scenarios. Note that each scenario is identified by a fault rupture plane and by a magnitude value, while a rupture realization refers to a particular slip distribution (and corresponding parameters, such as rupture time and rise time) on the given fault plane.

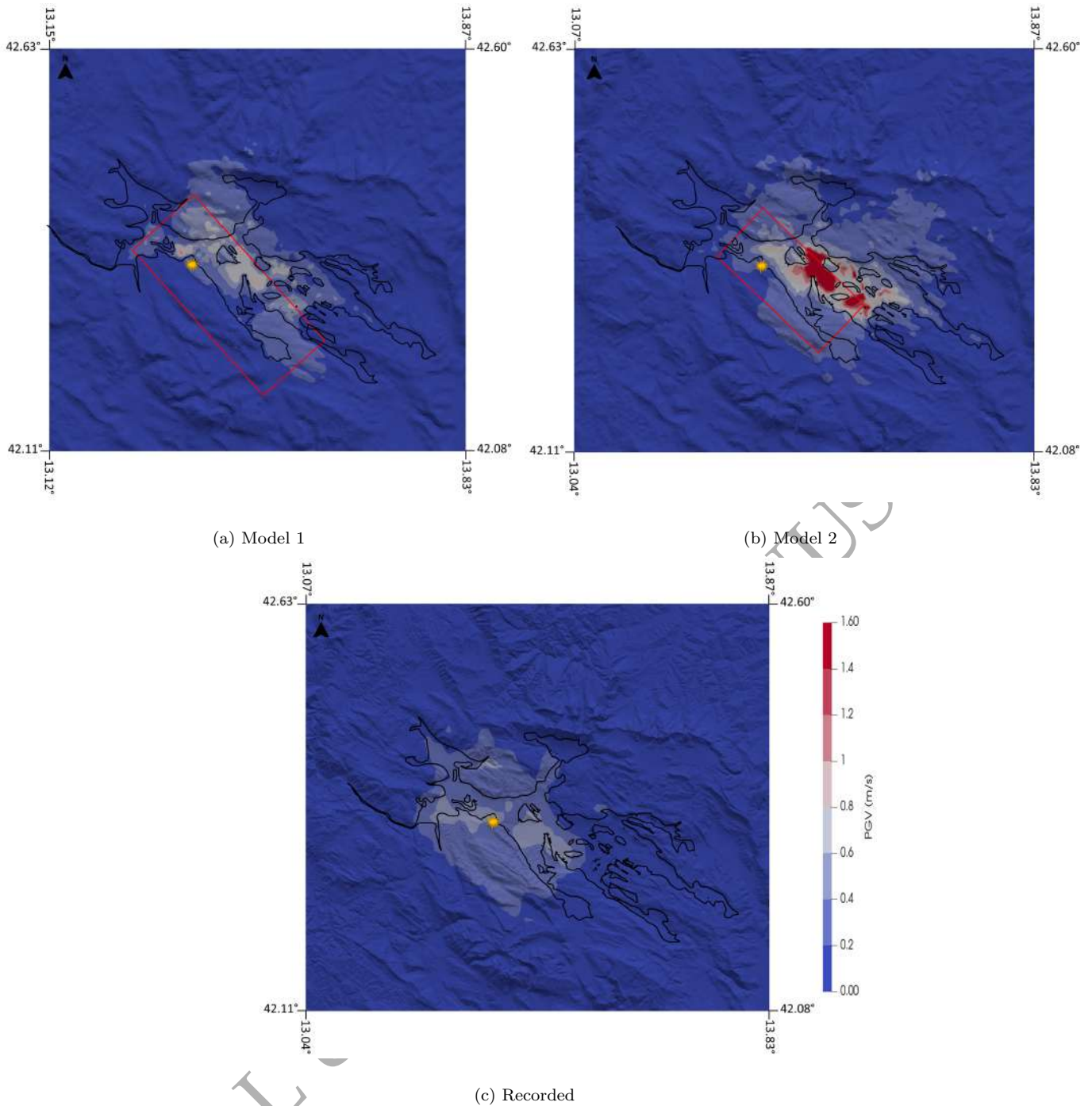


Figure 10. Comparison between PGV maps obtained from simulations *Model 1* (a) and *Model 2* (b), (c) shows the recorded data from shakemaps.

Starting from the 9 ground motion simulations, we computed the GoF scores by averaging the five metrics considered previously, i.e., ED, PGV, PGD, RS and FAS, for the three different components of the considered field. Figure 12 shows the score as a function of the considered earthquake scenario for Mw 6.1 (12-(a)), Mw 6.2 (12-(b)) and Mw 6.3 (12-(c)) and rupture realization (referred to as SC1, SC2 and SC3, for each magnitude).

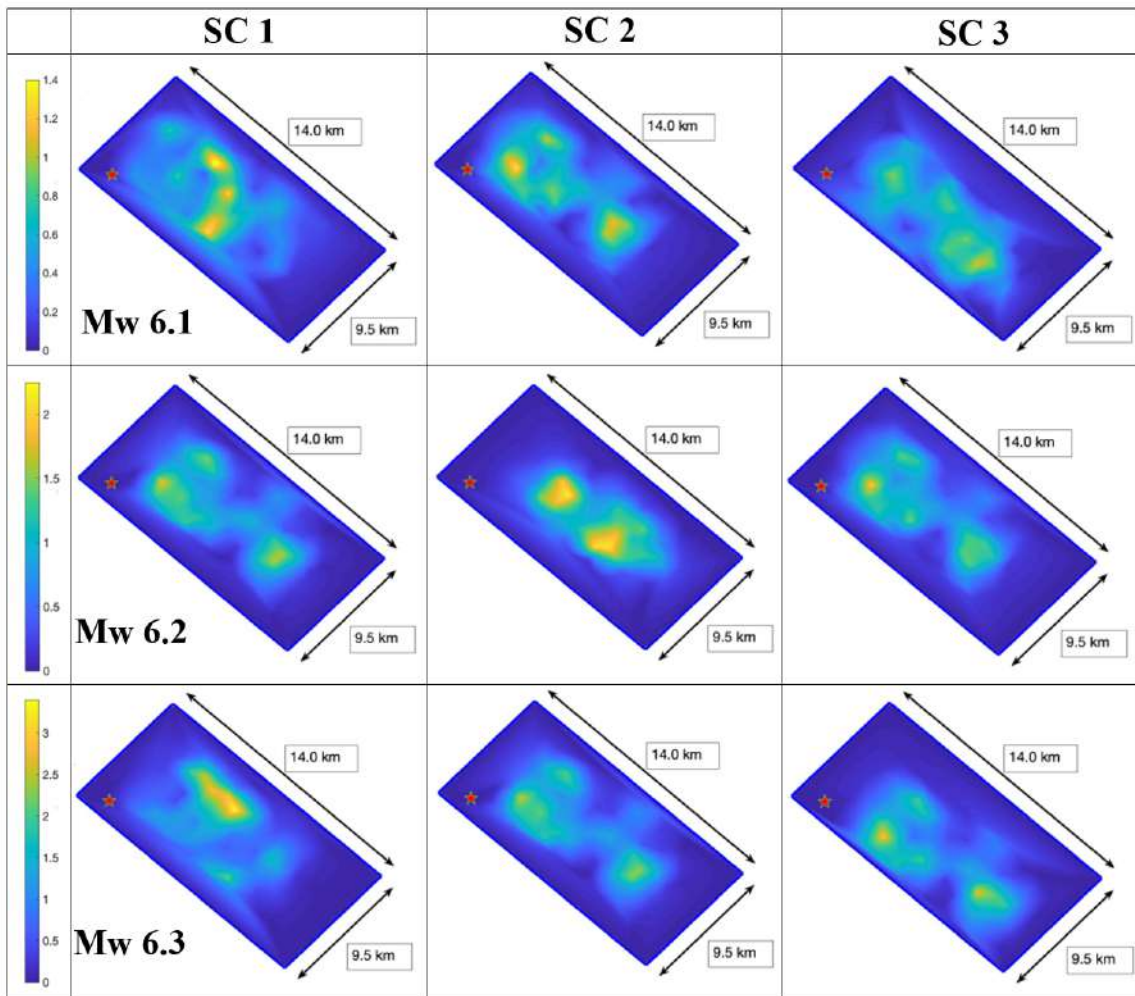


Figure 11. Slip distributions obtained using the rupture generator model developed in Schmedes et al. (2013)

As one can see, the scenarios that produced the best average GoF score, of around 5.5, are the scenarios Mw6.2-SC3 and Mw6.3-SC1. For these two scenarios, in Figure 13 the comparison between the three-component recorded and simulated waveforms are shown at AQK, AQU and AQG stations. In each of the three scenarios the stations AQV, AQG and AQA produce relatively low fit scores, this is likely due to an incomplete geological description of that region. To improve the result in this sense a lower scale model is needed. Note that, in each of the three scenarios, the stations AQV, AQG and AQA produce relatively low fit scores, most likely due to a combined effect of the source model, radiating limited energy in the

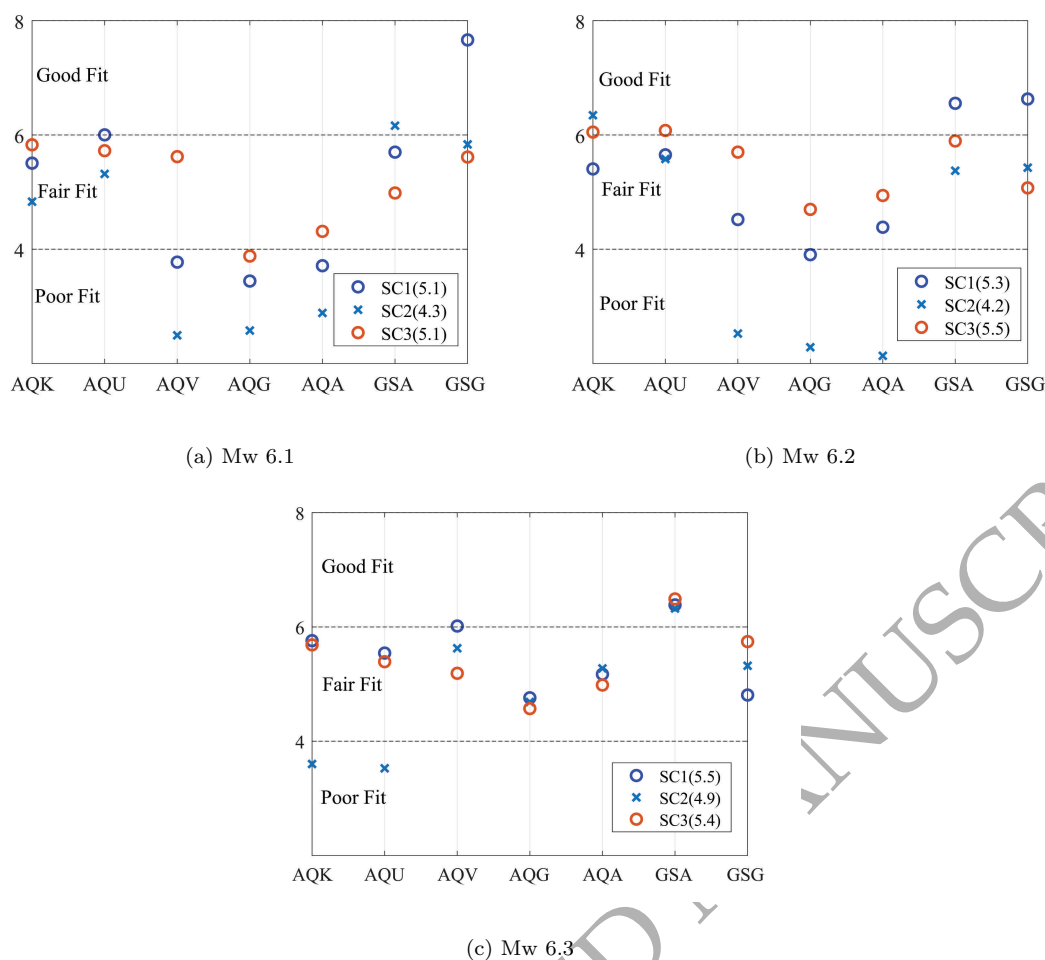


Figure 12. Average GoF value of the five metrics for all the stations under consideration for the scenario with Mw 6.1 (a), Mw 6.2 (b) and Mw 6.3 (c) in the frequency range [0.1, 2.5] Hz.

West direction regardless of the adopted slip distribution, and of deficiencies in the local site response model.

In general, the agreement is satisfactory, in particular for the stations closest to the epicenter (AQA and AQU) for both scenarios. At AQG the displacement time history is quite well reproduced in the EW and UD components especially in terms of peak values. The velocity, however, is strongly underestimated except for the UP direction. These misfits turn out to be stronger than the ones observed for the source models specifically calibrated on the L'Aquila observations, namely *Model 1* and *Model 2*. This suggests that the source, rather than approximations in the domain reconstruction, plays a major role in this analysis. Finally, we further analyze the Mw6.2-SC3 scenario, as it seems to reproduce more effectively the observed data at AQA and AQU stations.

The considered source is able to reproduce the up-dip rupture mechanism in a satisfactory way, see Figure 14, but, as shown in Figure 15, the observed co-seismic displacement is strongly underestimated, likely due to assumptions of the random

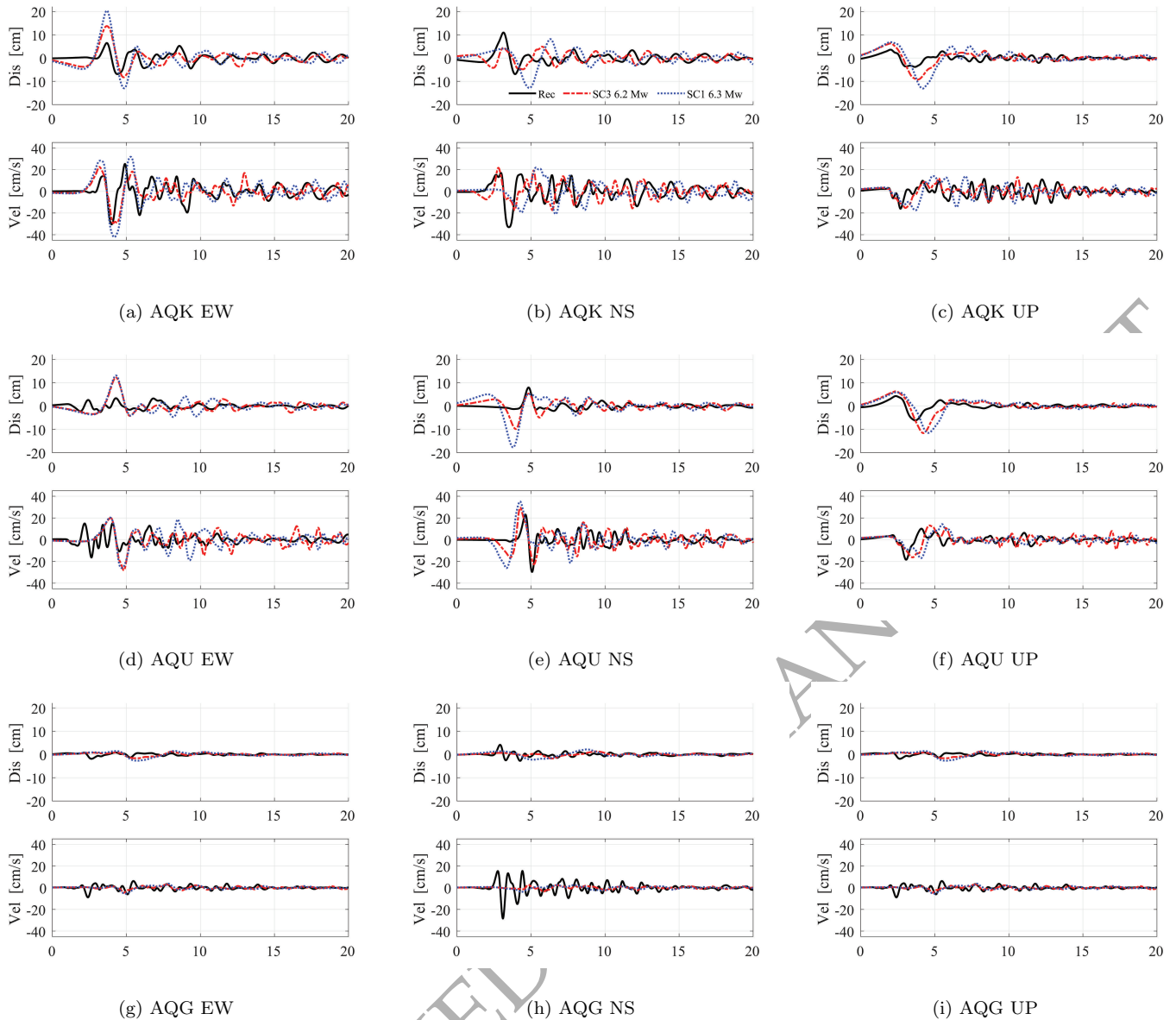


Figure 13. Comparison between recorded (black lines) and simulated waveforms for the stations AQQ, AQU and AQQ, in the frequency range $[0.1, 2.5]$ Hz for scenarios Mw6.2-SC3 (red lines) and Mw6.3-SC1 (blue lines).

source. A better result could be obtained by a wider set of earthquake scenarios and by considering the average value of the computed co-seismic displacement. This however is beyond the scope of this work.

Finally, we compare the simulated PGV map from scenario Mw6.2-SC3 with the ShakeMaps for the L'Aquila mainshock provided in (<http://shakemap.ingv.it/shake/archive/>), see figure 16. Although there is a general agreement between the two maps, it is quite clear that the simulated ground shaking map includes a small-scale spatial variability which cannot be reproduced by the ShakeMap approach. Such a variability is related to the details of the alluvial basin coupled with those of the fault rupture process. It is noted that in the simulated map higher PGV values are obtained, especially in the SE direction,

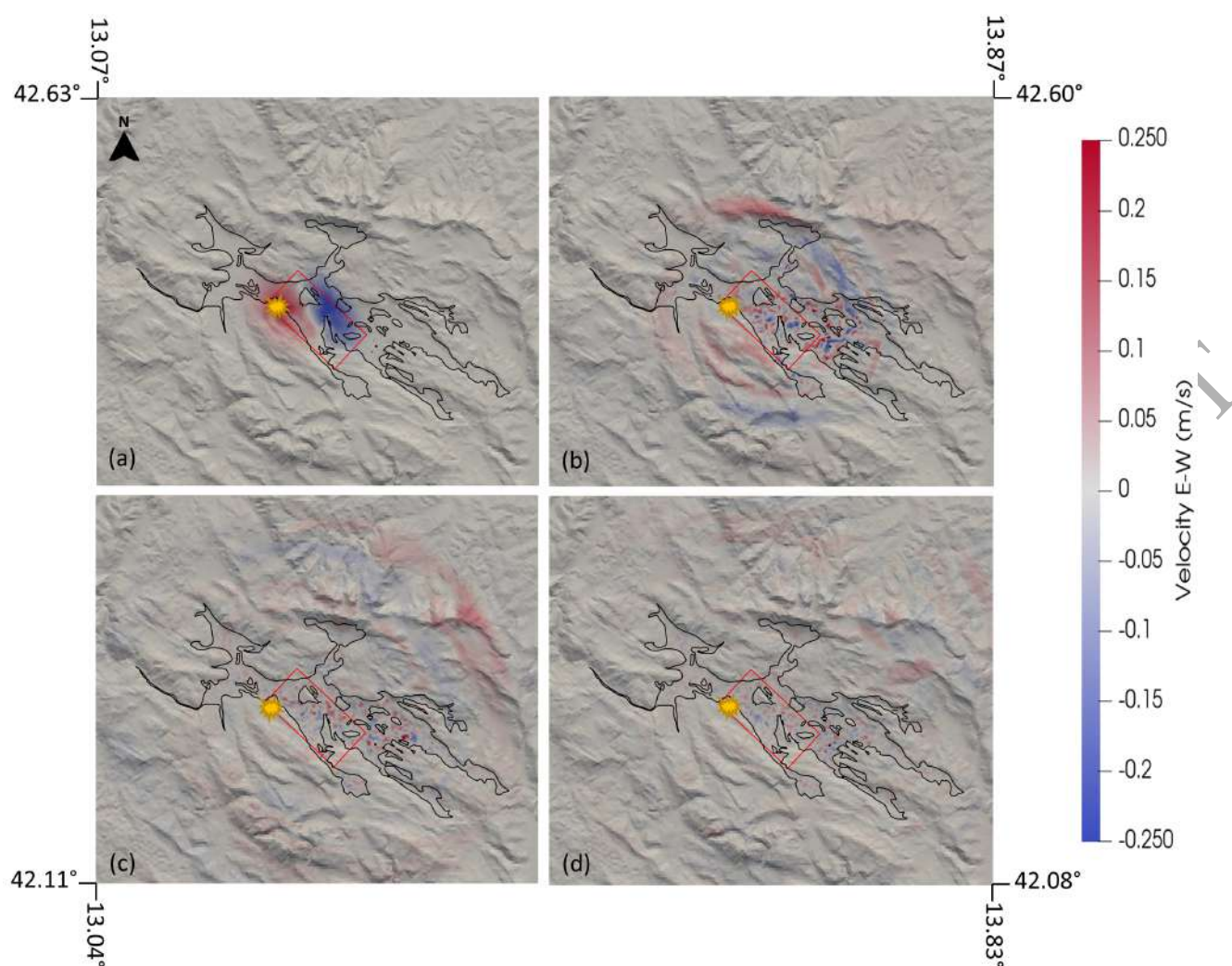


Figure 14. Snapshots of the velocity field in the EW direction for scenario Mw 6.2-SC3 at time 3.5 (a), 7.5 (b), 13.5 (c) and 17.5 s (d).

likely owing to the interaction of source directivity with the response of the basin where the sediments are of considerable thickness (see Figure 1).

Although the number of simulations is not sufficient for a robust statistical analysis, Figure 17 shows the mean and the standard deviation of the PGV, NS component, calculated considering all scenarios. As expected higher values of standard deviation can be found within the deeper part of the basin on the surface projection of the causative fault, where the effects of the extended source couple with those of complex (3D) local site amplification. In this region the value of the standard deviation reaches 20 cm/s in some localized areas. This observation is confirmed by looking at the time histories recorded at AQK (see Figure 18a). As a matter of fact, the nine scenarios show a different trend from each other, and also with respect to the recorded signal. A lower variability is observed instead in correspondence of seismic station GSA (18b), located on outcropping bedrock and farther from the source.

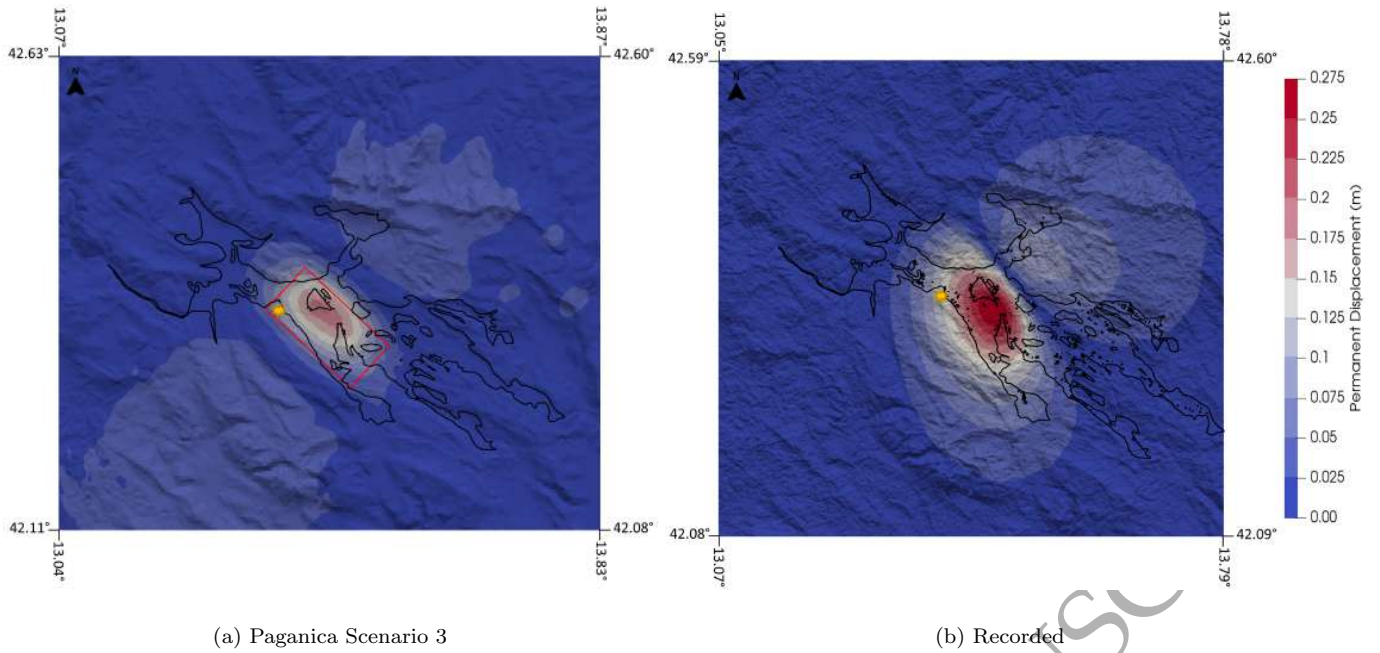


Figure 15. Permanent displacement registered after 30s for the the third scenario 6.2 Mw (a) compared to the coseismic displacement obtained by satellite data (b) (courtesy of Simone Atzori)

5 CONCLUSIONS AND FUTURE WORKS

In this paper we simulated the the April 6, 2009 L’Aquila earthquake using the numerical library SPEED. Our results show the importance of a well-constrained kinematic source model for near-source ground motion prediction. From this study, it turns

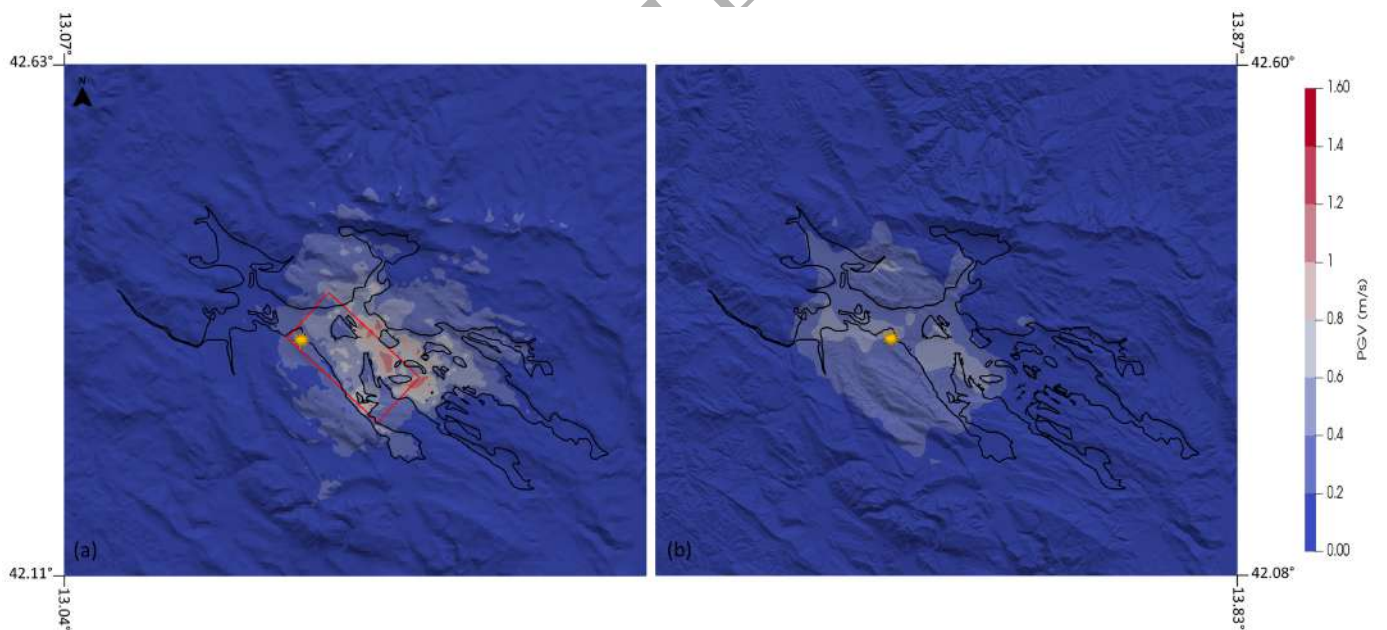


Figure 16. Comparison between simulated (a) PGV map (Mw 6.2-SC3) and ShakeMap (b) from <http://shakemap.ingv.it/shake/archive/>.

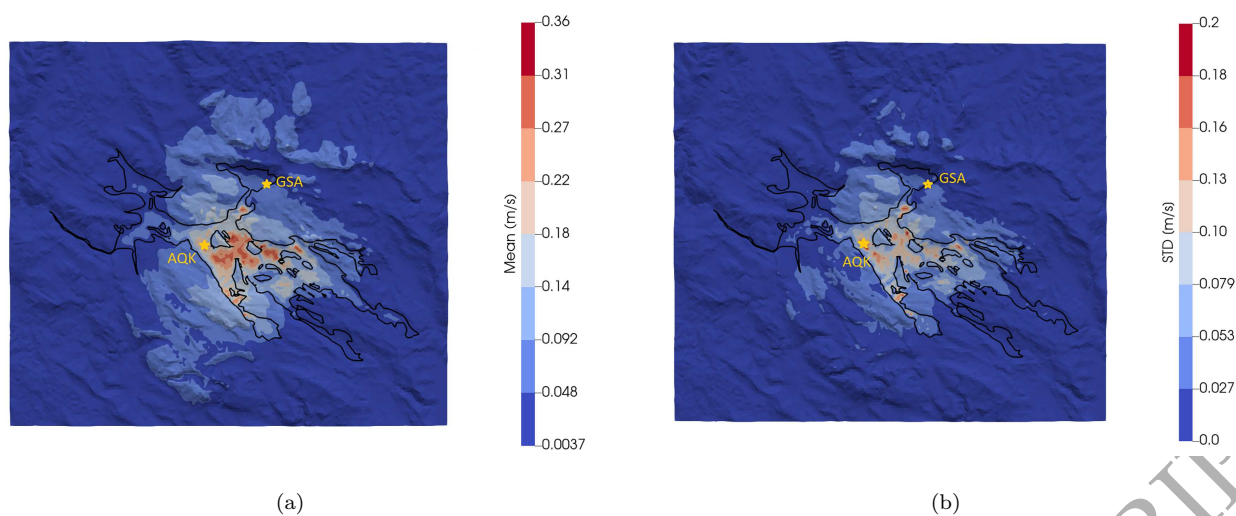


Figure 17. Mean value (a) and standard deviation (b) of the PGV, NS component, across the 9 scenarios.

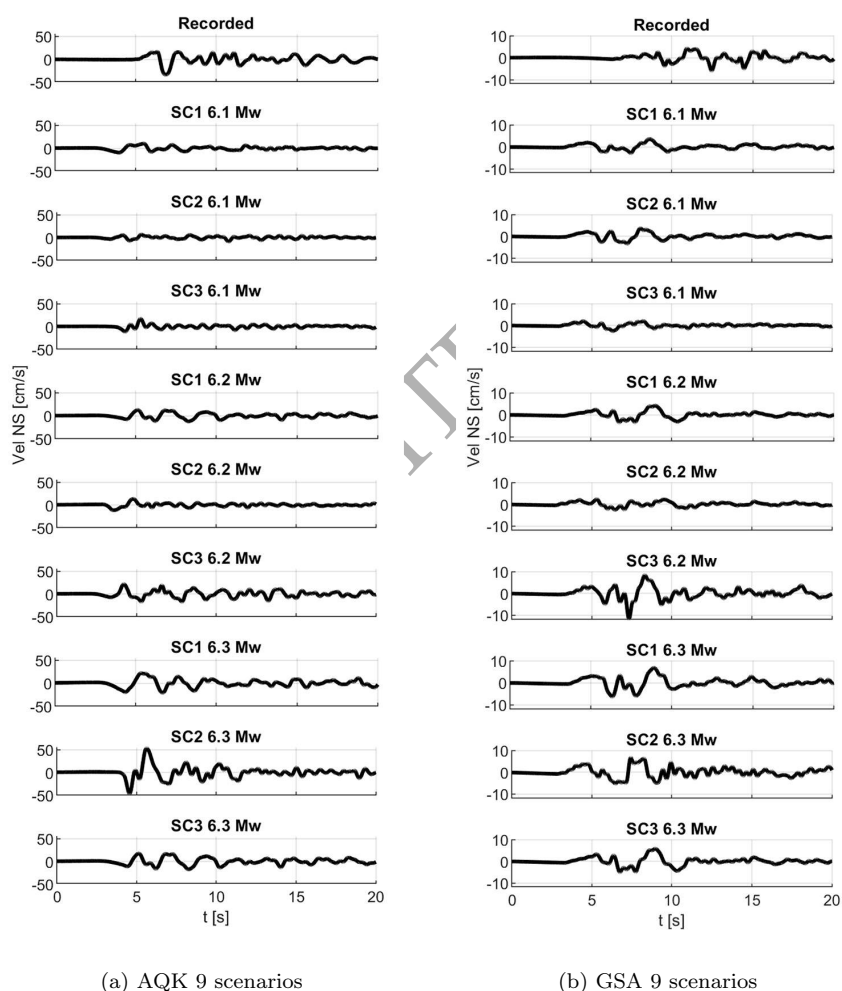


Figure 18. Comparison between the NS velocity component of recorded signal and of the 9 simulated scenarios. Two receivers are considered, namely AQK (a) and GSA (b), corresponding to a high and low value of standard deviation, respectively (see Figure 17b).

out that the best-fitting source model is the one proposed in Ameri et al. (2012) (*Model 1*), in agreement with previous studies on 3D physics-based simulations of L'Aquila earthquake. Besides the source model, we also show that a careful and detailed reconstruction of the geology and morphology of the area appears decisive for the accuracy of the obtained results. The results of this study are in satisfactory agreement with the observed ground motion features, especially for *Model 1*, where the average GoF is contained in the good fit region (cf Figure 8 (c)). Moreover, performing a blind prediction test, we show that it is possible to simulate an earthquake with acceptable accuracy, with a minimal set of input data on the target seismic event. The sensitivity of the prediction capability of simulated ground shaking scenarios with respect to the uncertainty of selected source parameters (such as the slip distribution) is a key aspect in ground motion prediction and it will be investigated in greater detail in future studies. Our work suggests that, given an accurate reconstruction of the topography and underlying geology, it is possible to obtain ground shaking scenarios with realistic features, i.e., comparable to the recorded motions, relying on some basic data on the seismic event. The latter include the target magnitude, the hypocentral depth - which typically ranges between 7 – 10 km for crustal earthquakes in the Apennine region - and the causative fault, which is constrained by accredited databases (such as DISS). Although a rigorous statistical analysis has not been carried out, the results of this study suggest the potential use of physics-based ground shaking scenarios for generating real-time ground shaking scenarios, with relevant implications for civil protection. A more extended study, including the generation of broadband ground motions over a wider domain (including other geological structures besides the Aterno Valley), will be the subject of a future work. Furthermore, in future analyses, the influence of the anisotropy and heterogeneity of the Earth crustal model will be also addressed.

6 ACKNOWLEDGEMENTS

This paper is part of a larger project focused on the post-earthquake reconstruction of the city of L'Aquila (see <https://www.opendatalaquila.it>).

This work was partially supported by the GNCS-INdAM and the GSSI "Centre for Urban Informatics and Modelling" (CUIM).

All numerical simulations have been realized on the Linux HPC cluster Caliban of the High Performance Parallel Computing Laboratory of the Department of Information Engineering, Computer Science and Mathematics (DISIM) at the University of L'Aquila (<https://caliband.disim.univaq.it>), employing the software SPEED <http://speed.mox.polimi.it>. We thank

the DISIM for the technical support. We also thank Dr. Simone Atzori (INGV) for the DInSAR data on the permanent displacement maps. Domains were partly constructed using Leapfrog (<https://www.seequent.com/products-solutions/leapfrog-geo/>

[Seequent (2019)]].

I.M., P.F.A. and A.Q. are members of INdAM-GNCS, B.R. and P.M. are members of INdAM-GNAMPA. F.DiM., R.A. and P.M. are members of GSSI-CUIM research center. We also thank the two anonymous referees and the associate editor for the constructive remarks.

DATA AVAILABILITY

Numerical models and results will be available at the website <https://www.opendatalaquila.it>.

References

- Ameri, G., Massa, M., Bindi, D., D'Alema, E., Gorini, A., Luzi, L., Marzorati, S., Pacor, F., Paolucci, R., Puglia, R., et al., 2009. The 6 April 2009 Mw 6.3 L'Aquila (central Italy) earthquake: strong-motion observations, *Seism. Res. Lett.*, **80**(6), 951–966.
- Ameri, G., Gallovič, F., & Pacor, F., 2012. Complexity of the Mw 6.3 2009 L'Aquila (central Italy) earthquake: 2. Broadband strong motion modeling, *J. Geophys. Res. Solid Earth*, **117**(B4).
- Anderson, J. G., 2004. Quantitative measure of the goodness-of-fit of synthetic seismograms, in *Proceedings of the 13th World Conference on Earthquake Engineering*, p. 243, International Association for Earthquake Engineering.
- Antonietti, P. F., Mazzieri, I., Quarteroni, A., & Rapetti, F., 2012. Non-conforming high order approximations of the elastodynamics equation, *Comput. Methods in Appl. Mech. Eng.*, **209**, 212–238.
- Antonietti, P. F., Ayuso de Dios, B., Mazzieri, I., & Quarteroni, A., 2016. Stability Analysis of Discontinuous Galerkin approximations to the elastodynamics problem, *J. Sci. Comput.*, **68**, 143–170.
- Antonietti, P. F., Ferroni, A., Mazzieri, I., Paolucci, R., Quarteroni, A., Smerzini, C., & Stupazzini, M., 2018. Numerical modeling of seismic waves by discontinuous spectral element methods, *ESAIM: Proceedings and Surveys*, **61**, 1–37.
- Asimaki, D. & Mohammadi, K., 2018. On the complexity of seismic waves trapped in irregular topographies, *Soil Dynamics and Earthquake Engineering*, **114**, 424–437.
- Assimaki, D., Ledezma, C., Montalva, G. A., Tassara, A., Mylonakis, G., & Boroschek, R., 2012. Site effects and damage patterns, *Earthq. Spectra*, **28**(S1), S55–S74.
- Atzori, S., Hunstad, I., Chini, M., Salvi, S., Tolomei, C., Bignami, C., Stramondo, S. E., Trasatti, E., Antonioli, A., & Boschi, E., 2009. Finite fault inversion of DInSAR coseismic displacement of the 2009 L'Aquila earthquake (central Italy), *Geophys. Res. Lett.*, **36**(15).
- Avallone, A., Marzario, M., Cirella, A., Piatanesi, A., Rovelli, A., Di Alessandro, C., D'Anastasio, E., D'Agostino, N., Giuliani, R., & Mattone, M., 2011. Very high rate (10 Hz) GPS seismology for moderate-magnitude earthquakes: The case of the Mw 6.3 L'Aquila (central Italy) event, *J. Geophys. Res. Solid Earth*, **116**(B2).
- Balasco, M., Galli, P., Giocoli, A., Gueguen, E., Lapenna, V., Perrone, A., Piscitelli, S., Rizzo, E., Romano, G., Siniscalchi, A., et al., 2011. Deep geophysical electromagnetic section across the middle Aterno Valley (central Italy): preliminary results after the April 6, 2009 L'Aquila earthquake, *Boll. di Geofis. Teor. ed Appl.*, **52**(3), 443–455.

- Bard, P. & Bouchon, M., 1980. The seismic response of sediment-filled valleys. Part 1. The case of incident SH waves, *Bull. seism. Soc. Am.*, **70**(4), 1263–1286.
- Bertini, T. & Bosi, C., 1976. Sedimenti continentali probabilmente Pliocenici nella Valle del Salto e nella Conca del Fucino (Rieti e l'Aquila).
- Bertini, T. & Bosi, C., 1993. La tettonica quaternaria della conca di Fossa (L'Aquila), *Il Quaternario*, **6**(2), 293–314.
- Bielak, J., Graves, R. W., Olsen, K. B., Taborda, R., Ramírez-Guzmán, L., Day, S. M., Ely, G. P., Roten, D., Jordan, T. H., Maechling, P. J., et al., 2010. The ShakeOut earthquake scenario: Verification of three simulation sets, *Geophys. J. Int.*, **180**(1), 375–404.
- Bosi, C., 1989. Tentativo di correlazione fra le successioni plio-pleistoceniche, *Elementi di tettonica pliocenico-quaternaria e indizi di sismicità olocenica nell'Appennino laziale-abruzzese*, pp. 89–96.
- Bosi, C. & Bertini, T., 1970. Geologia della media valle dell'Aterno, *Mem. Soc. Geol. It.*, **9**(4), 719–777.
- Bouchon, M. & Barker, J. S., 1996. Seismic response of a hill: the example of Tarzana, California, *Bull. seism. Soc. Am.*, **86**(1A), 66–72.
- Bouchon, M., Schultz, C. A., & Toksöz, M., 1996. Effect of three-dimensional topography on seismic motion, *J. Geophys. Res. Solid Earth*, **101**(B3), 5835–5846.
- Breuer, A., Heinecke, A., Rettenberger, S., Bader, M., Gabriel, A.-A., & Pelties, C., 2014. Sustained petascale performance of seismic simulations with seissol on supermuc, in *International Supercomputing Conference*, pp. 1–18, Springer.
- Burstedde, C., Stadler, G., Alisic, L., Wilcox, L. C., Tan, E., Gurnis, M., & Ghattas, O., 2013. Large-scale adaptive mantle convection simulation, *Geophys. J. Int.*, **192**(3), 889–906.
- Carafa, M. & Bird, P., 2016. Improving deformation models by discounting transient signals in geodetic data: 2. Geodetic data, stress directions, and long-term strain rates in Italy, *J. Geophys. Res. Solid Earth*, **121**(7), 5557–5575.
- Carafa, M., Valensise, G., & Bird, P., 2017. Assessing the seismic coupling of shallow continental faults and its impact on seismic hazard estimates: a case-study from Italy, *Geophys. J. Int.*, **209**(1), 32–47.
- Carafa, M., Galvani, A., Di Naccio, D., Kastelic, V., Di Lorenzo, C., Miccolis, S., Sepe, V., Pietrantonio, G., Gizzi, C., Massucci, A., Galadini, F., Valensise, G., & Bird, P., 2020. Partitioning the ongoing extension of the central Apennines (Italy): fault slip rates and bulk deformation rates from geodetic and stress data, *J. Geophys. Res. Solid Earth*, **in press**.
- Centamore, E., U., & Dramis, F., 2010. Note illustrative della Carta Geologica d'Italia alla scala 1:50.000, Foglio 358- Pescorocchiano. ISPRA-Servizio Geologico d'Italia, Ente realizzatore Regione Lazio.
- Chaljub, E., Maufroy, E., Moczo, P., Kristek, J., Hollender, F., Bard, P.-Y., Priolo, E., Klin, P., de Martin, F., Zhang, Z., Zhang, W., & Chen, X., 2015. 3-D numerical simulations of earthquake ground motion in sedimentary basins: testing accuracy through stringent models, *Geophys. J. Int.*, **201**(1), 90–111.
- Cheloni, D., D'agostino, N., D'anastasio, E., Avallone, A., Mantenuto, S., Giuliani, R., Mattone, M., Calcaterra, S., Gambino, P., Dominici, D., et al., 2010. Coseismic and initial post-seismic slip of the 2009 Mw 6.3 l'Aquila earthquake, Italy, from GPS measurements, *Geophys. J. Int.*, **181**(3), 1539–1546.
- Cirella, A., Piatanesi, A., Cocco, M., Tinti, E., Scognamiglio, L., Michelini, A., Lomax, A., & Boschi, E., 2009. Rupture history of the

- 2009 L'Aquila (Italy) earthquake from non-linear joint inversion of strong motion and GPS data, *Geophys. Res. Lett.*, **36**(19).
- Cosentino, D., Asti, R., Nocentini, M., Gliozzi, E., Kotsakis, T., Mattei, M., Esu, D., Spadi, M., Tallini, M., Cifelli, F., et al., 2017. New insights into the onset and evolution of the central Apennine extensional intermontane basins based on the tectonically active L'Aquila Basin (central Italy), *Bulletin*, **129**(9-10), 1314–1336.
- De Luca, G., Marcucci, S., Milana, G., & Sano, T., 2005. Evidence of low-frequency amplification in the city of L'Aquila, Central Italy, through a multidisciplinary approach including strong-and weak-motion data, ambient noise, and numerical modeling, *Bull. seism. Soc. Am.*, **95**(4), 1469–1481.
- Della Seta, M., Esposito, C., Marmoni, G. M., Martino, S., Mugnozza, G. S., & Troiani, F., 2017. Morpho-structural evolution of the valley-slope systems and related implications on slope-scale gravitational processes: New results from the Mt. Genzana case history (Central Apennines, Italy), *Geomorphology*, **289**, 60–77.
- Dipartimento Difesa del Suolo, 2005a. APAT (2005a), Italian Geological Map, sheet n° 368 "Avezzano", scale 1:50,000.
- Dipartimento Difesa del Suolo, 2005b. APAT (2005b), Italian Geological Map, sheet n° 368 "L'Aquila", scale 1:50,000.
- Dipartimento Difesa del Suolo, 2005c. APAT (2005c), Italian Geological Map, sheet n° 368 "Torre dei passerii", scale 1:50,000.
- Dumbser, M., Käser, M., & Toro, E. F., 2007. An arbitrary high-order Discontinuous Galerkin method for elastic waves on unstructured meshes-V. Local time stepping and p -adaptivity, *Geophys. J. Int.*, **171**(2), 695–717.
- Durand, S., Gaffet, S., & Virieux, J., 1999. Seismic diffracted waves from topography using 3-D discrete wavenumber-boundary integral equation simulation, *Geophysics*, **64**(2), 572–578.
- Duru, K., Rannabauer, L., Gabriel, A.-A., Kreiss, G., & Bader, M., 2020. A stable discontinuous galerkin method for the perfectly matched layer for elastodynamics in first order form, *Numerische Mathematik*, **146**(4), 729–782.
- Evangelista, L., Del Gaudio, S., Smerzini, C., d'Onofrio, A., Festa, G., Iervolino, I., Landolfi, L., Paolucci, R., Santo, A., & Silvestri, F., 2017. Physics-based seismic input for engineering applications: a case study in the Aterno river valley, Central Italy, *Bull. Earth. Eng.*, **15**(7), 2645–2671.
- Ewald, M., Igel, H., Hinzen, K.-G., & Scherbaum, F., 2006. Basin-related effects on ground motion for earthquake scenarios in the lower rhine embayment, *Geophysical Journal International*, **166**(1), 197–212.
- Ferroni, A., Antonietti, P. F., Mazzieri, I., & Quarteroni, A., 2017. Dispersion-dissipation analysis of 3-D continuous and discontinuous spectral element methods for the elastodynamics equation, *Geophys. J. Int.*, **211**, 1554–1574.
- Gallipoli, M. R., Gizzi, F. T., Rizzo, E., Masini, N., Potenza, M. R., Albarello, D., & Lapenna, V., 2012. Site features responsible for uneven seismic effects in historical centre of Melfi (Basilicata, Southern Italy), *Disaster Adv.*, **5**(3), 125–137.
- Galvez, P., Ampuero, J.-P., Dalguer, L. A., Somala, S. N., & Nissen-Meyer, T., 2014. Dynamic earthquake rupture modelled with an unstructured 3-D spectral element method applied to the 2011 M9 Tohoku earthquake, *Geophys. J. Int.*, **198**(2), 1222–1240.
- Giacco, B., Galli, P., Messina, P., Peronace, E., Scardia, G., Sottili, G., Sposato, A., Chiarini, E., Jicha, B., & Silvestri, S., 2012. Fault and basin depocentre migration over the last 2 Ma in the L'Aquila 2009 earthquake region, central Italian Apennines, *Quat. Sci. Rev.*, **56**, 69–88.
- Guidoboni, E., Ferrari, G., Tarabusi, G., Sgattoni, G., Comastri, A., Mariotti, D., Ciuccarelli, C., Bianchi, M. G., & Valensise, G., 2019.

- CFTI5Med, the new release of the catalogue of strong earthquakes in Italy and in the Mediterranean area, *Sci. Data*, **6**(1), 1–15.
- Gutenberg, B., 1957. Effects of ground on earthquake motion, *Bulletin of the Seismological Society of America*, **47**(3), 221–250.
- Hailemikael, S., Lenti, L., Martino, S., Paciello, A., Rossi, D., & Mugnozsa, G. S., 2016. Ground-motion amplification at the colle di roio ridge, central italy: a combined effect of stratigraphy and topography, *Geophysical Journal International*, **206**(1), 1–18.
- Improta, L., Villani, F., Bruno, P. P., Castiello, A., De Rosa, D., Varriale, F., Punzo, M., Brunori, C. A., Civico, R., Pierdominici, S., et al., 2012. High-resolution controlled-source seismic tomography across the Middle Aterno basin in the epicentral area of the 2009, Mw 6.3, L'Aquila earthquake (central Apennines, Italy), *Ital. J. Geosci.*, **131**(3), 373–388.
- Infantino, M., Mazzieri, I., Özcebe, A. G., Paolucci, R., & Stupazzini, M., 2020. 3D physics-based numerical simulations of ground motion in Istanbul from earthquakes along the marmara segment of the North Anatolian Fault, *Bull. seism. Soc. Am.*, **110**(5), 2559–2576.
- Kastelic, V., Burrato, P., Carafa, M., & Basili, R., 2017. Repeated surveys reveal nontectonic exposure of supposedly active normal faults in the central Apennines, Italy, *J. Geophys. Res. Earth Surf.*, **122**(1), 114–129.
- Kawase, H., 1996. The cause of the damage belt in Kobe: “The basin-edge effect,” constructive interference of the direct S-wave with the basin-induced diffracted/Rayleigh waves, *Seism. Res. Lett.*, **67**(5), 25–34.
- Komatitsch, D., Liu, Q., Tromp, J., Suss, P., Stidham, C., & Shaw, J. H., 2004. Simulations of ground motion in the los angeles basin based upon the spectral-element method, *Bulletin of the Seismological Society of America*, **94**(1), 187–206.
- Kotha, S. R., Weatherill, G., Bindi, D., & Cotton, F., 2020. A regionally-adaptable ground-motion model for shallow crustal earthquakes in Europe, *Bull. Earth. Eng.*.
- Lee, S. J., Komatitsch, D., Huang, B. S., & Tromp, J., 2009. Effects of topography on seismic-wave propagation: An example from northern Taiwan, *Bull. seism. Soc. Am.*, **99**(1), 314–325.
- Lovati, S., Bakavoli, M., Massa, M., Ferretti, G., Pacor, F., Paolucci, R., Haghshenas, E., & Kamalian, M., 2011. Estimation of topographical effects at narni ridge (central italy): comparisons between experimental results and numerical modelling, *Bulletin of earthquake Engineering*, **9**(6), 1987–2005.
- Macrì, P., Smedile, A., Speranza, F., Sagnotti, L., Porreca, M., Mochales, T., & Ermolli, E. R., 2016. Analysis of a 150 m sediment core from the co-seismic subsidence depocenter of the 2009 Mw= 6.1 L'Aquila earthquake (Italy): Implications for Holocene–Pleistocene tectonic subsidence rates and for the age of the seismogenic Paganica fault system, *Tectonophysics*, **687**, 180–194.
- Magnoni, F., Casarotti, E., Michelini, A., Piersanti, A., Komatitsch, D., Peter, D., & Tromp, J., 2013. Spectral-element simulations of seismic waves generated by the 2009 l'Aquila earthquake, *Bull. seism. Soc. Am.*, **104**(1), 73–94.
- Mancini, M., Cavuoto, G., Pandolfi, L., Petronio, C. and Salari, L., & Sardella, R., 2012. Coupling basin infill history and mammal biochronology in a Pleistocene intramontane basin: The case of western L'Aquila Basin (central Apennines, Italy), *Quaternary International*, **267**, 62–77.
- May, J., Pera, D., Di Michele, F., Rubino, B., Aloisio, R., & Marcati, P., 2021. Fast cubit python tool for highly accurate topography generation and layered domain reconstruction.
- Mazzieri, I., Stupazzini, M., Guidotti, R., & Smerzini, C., 2013. SPEED: SPectral Elements in Elastodynamics with Discontinuous

- Galerkin: A non-conforming approach for 3D multi-scale problems, *Int. J. Numer. Method Eng.*, **95**(12), 991–1010.
- Moczo, P., Kristek, J., Galis, M., Chaljub, E., & Etienne, V., 2011. 3-D finite-difference, finite-element, discontinuous-Galerkin and spectral-element schemes analysed for their accuracy with respect to P-wave to S-wave speed ratio, *Geophys. J. Int.*, **187**(3), 1645–1667.
- Moczo, P., Kristek, J., & Gális, M., 2014. *The Finite-Difference Modelling of Earthquake Motions: Waves and Ruptures*, Cambridge University Press.
- MS-AQ Working Group and others, 2010. Microzonazione sismica per la ricostruzione dell'area aquilana. 3 Vol.+ CD rom, *Regione Abruzzo—Dipartimento della Protezione Civile, L'Aquila (in Italian)*.
- Nocentini, M., Asti, R., Cosentino, D., Durante, F., Gliozzi, E., M., L., & Tallini, M., 2017. Plio-Quaternary geology of L'Aquila–Scoppito Basin (Central Italy), *J. Maps*, **13**(2), 563–574.
- Nocentini, M., Cosentino, D., Spadi, M., & Tallini, M., 2018. Plio-Quaternary geology of the Paganica-San Demetrio-Castelnuovo Basin (Central Italy), *J. Maps*, **14**(2), 411–420.
- Paolucci, R. & Smerzini, C., 2018. Empirical evaluation of peak ground velocity and displacement as a function of elastic spectral ordinates for design, *Earthquake Engineering & Structural Dynamics*, **47**(1), 245–255.
- Paolucci, R., Mazzieri, I., & Smerzini, C., 2015. Anatomy of strong ground motion: near-source records and three-dimensional physics-based numerical simulations of the Mw 6.0 2012 May 29 Po Plain earthquake, Italy, *Geophys. J. Int.*, **203**(3), 2001–2020.
- Paolucci, R., Evangelista, L., Mazzieri, I., & Schiappapietra, E., 2016. The 3D numerical simulation of near-source ground motion during the Marsica earthquake, central Italy, 100 years later, *Soil Dyn. Earthq. Eng.*, **91**, 39 – 52.
- Paolucci, R., Mazzieri, I., Piuanno, G., Smerzini, C., Vanini, M., & Özcebe, A. G., 2021a. Earthquake ground motion modeling of induced seismicity in the Groningen gas field, *Earthquake Eng. Struct. Dynam.*, **50**(1), 135–154.
- Paolucci, R., Smerzini, C., & Vanini, M., 2021b. BB-SPEEDset: A Validated Dataset of Broadband Near-Source Earthquake Ground Motions from 3D Physics-Based Numerical Simulations, *Bulletin of the Seismological Society of America*.
- Patacca, E. & Scandone, P., 1989. Post-Tortonian mountain building in the Apennines. The role of the passive sinking of a relic lithospheric slab.
- Pelties, C., Puente, J., Ampuero, J.-P., Brietzke, G., & Käser, M., 2012. Three-dimensional dynamic rupture simulation with a high-order discontinuous Galerkin method on unstructured tetrahedral meshes, *J. Geophys. Res. Solid Earth*, **117**(B2).
- Peter, D., Komatitsch, D., Luo, Y., Martin, R., Le Goff, N., Casarotti, E., Le Loher, P., Magnoni, F., Liu, Q., Blitz, C., et al., 2011. Forward and adjoint simulations of seismic wave propagation on fully unstructured hexahedral meshes, *Geophysical Journal International*, **186**(2), 721–739.
- Petersson, N. A. & Sjögreen, B., 2018. High Order Accurate Finite Difference Modeling of Seismo-Acoustic Wave Propagation in a Moving Atmosphere and a Heterogeneous Earth Model Coupled Across a Realistic Topography, *J. Sci. Comput.*, **74**(1), 209–323.
- Porreca, M., Smedile, A., Speranza, F., Mochales, T., Caracciolo, F. D., Di Giulio, G., Vassallo, M., Villani, F., Nicolosi, I., Carluccio, R., et al., 2016. Geological reconstruction in the area of maximum co-seismic subsidence during the 2009 Mw= 6.1 L'Aquila earthquake using geophysical and borehole data, *Ital. J. Geosci.*, **135**(2), 350–362.
- Pucci, S., Civico, R., Villani, F., Ricci, T., Delcher, E., Finizola, A., Sapia, V., De Martini, P. M., Pantosti, D., Barde-Cabusson, S.,

- et al., 2016. Deep electrical resistivity tomography along the tectonically active Middle Aterno Valley (2009 L'Aquila earthquake area, central Italy), *Geophys. J. Int.*, **207**(2), 967–982.
- Rovida, A., Locati, M., Camassi, R., Lolli, B., & Gasperini, P., 2019. Catalogo Parametrico dei Terremoti Italiani (CPTI15), versione 2.0.
- Schmedes, J., Archuleta, R. J., & Lavallée, D., 2013. A kinematic rupture model generator incorporating spatial interdependency of earthquake source parameters, *Geophys. J. Int.*, **192**(3), 1116–1131.
- Seequent, 2019. Leapfrog Geo.
- Servizio Geologico d'Italia, 2010a. ISPRA (2010a), Italian Geological Map, sheet n 358 Pescocochiano", scale 1:50,000.
- Servizio Geologico d'Italia, 2010b. ISPRA (2010b), Italian Geological Map, sheet n 349 "Gran Sasso d'Italia", scale 1:50,000.
- Sgobba, S., Lanzano, G., & Pacor, F., 2021. Empirical nonergodic shaking scenarios based on spatial correlation models: An application to central Italy, *Earthquake Eng. Struct. Dynam.*, **50**(1), 60–80.
- Smerzini, C. & Villani, M., 2012. Broadband numerical simulations in complex near-field geological configurations: The case of the 2009 Mw 6.3 L'Aquila earthquake, *Bull. seism. Soc. Am.*, **102**(6), 2436–2451.
- Stupazzini, M., Paolucci, R., & Igel, H., 2009. Near-fault earthquake ground-motion simulation in the Grenoble valley by a high-performance spectral element code, *Bull. seism. Soc. Am.*, **99**(1), 286–301.
- Sugan, M., Kato, A., Miyake, H., Nakagawa, S., & Vuan, A., 2014. The preparatory phase of the 2009 Mw 6.3 L'Aquila earthquake by improving the detection capability of low-magnitude foreshocks, *Geophys. Res. Lett.*, **41**(17), 6137–6144.
- Tallini, M., Cavuoto, G., Del Monaco, F., Di Fiore, V., Mancini, M., Caielli, G., Cavinato, G., De Franco, R., Pelosi, N., & Rapolla, A., 2012. Seismic surveys integrated with geological data for in-depth investigation of Mt. Pettino active Fault area (Western L'Aquila Basin), *Ital. J. Geosci.*, **131**(3), 389–402.
- Tarquini, S. & Nannipieri, L., 2017. The 10 m-resolution TINITALY DEM as a trans-disciplinary basis for the analysis of the Italian territory: Current trends and new perspectives, *Geomorphology*, **281**, 108–115.
- Tarquini, S., Isola, I., Favalli, M., Mazzarini, F., Bisson, M., Pareschi, M. T., & Boschi, E., 2007. TINITALY/01: a new triangular irregular network of Italy, *Ann. Geophys.*
- Tarquini, S., Vinci, S., Favalli, M., Doumaz, F., Fornaciai, A., & Nannipieri, L., 2012. Release of a 10-m-resolution DEM for the Italian territory: Comparison with global-coverage DEMs and anaglyph-mode exploration via the web, *Comput. Geosci.*, **38**(1), 168–170.
- Tromp, J., Komatitsch, D., & Liu, Q., 2008. Spectral-element and adjoint methods in seismology, *Communications in Computational Physics*, **3**(1), 1–32.
- van Zelst, I., Wollherr, S., Gabriel, A.-A., Madden, E. H., & van Dinther, Y., 2019. Modeling Megathrust Earthquakes Across Scales: One-way Coupling From Geodynamics and Seismic Cycles to Dynamic Rupture, *J. Geophys. Res. Solid Earth*, **124**(11), 11414–11446.
- Vezzani, L., Ghisetti, F., Bigozzi, A., Follador, U., & Casnedi, R., 1998. *Carta geologica dell'Abruzzo: scala 1: 100.000*, Selca.
- Wolf, S., Gabriel, A.-A., & Bader, M., 2020. Optimization and local time stepping of an ader-dg scheme for fully anisotropic wave propagation in complex geometries, in *International Conference on Computational Science*, pp. 32–45, Springer.
- Yano, T. E., Shao, G., Liu, Q., Ji, C., & Archuleta, R. J., 2014. Coseismic and potential early afterslip distribution of the 2009 Mw 6.3

L'Aquila, Italy earthquake, *Geophys. J. Int.*, **199**(1), 23–40.

Zambonelli, E., de Nardis, R., Filippi, L., Nicoletti, M., & Dolce, M., 2017. Performance of the Italian strong motion network during the 2009, L'Aquila seismic sequence (central Italy), *Geomorphology*, **281**, 108–115.

ORIGINAL UNEDITED MANUSCRIPT